Experimental Investigation of Swirl Flow in a Ribbed Cylindrical Container using Particle Image Velocimetry

By

Tahir Javed

Reg. No. 00000277727

Session 2018-20

Supervised by

Dr. Majid Ali

US-Pakistan Center for Advanced Studies in Energy (USPCAS-E)

National University of Sciences and Technology (NUST)

H-12, Islamabad 44000, Pakistan

2022

Experimental Investigation of Swirl Flow in a Ribbed Cylindrical Container using Particle Image Velocimetry

By

Tahir Javed

Reg. No. 00000277727

Session 2018-20

Supervised by

Dr. Majid Ali

A Thesis Submitted to the US-Pakistan Center for Advanced Studies in Energy in partial fulfillment of the requirements for the degree of

MASTER of SCIENCE

in

THERMAL ENERGY ENGINEERING

US-Pakistan Center for Advanced Studies in Energy (USPCAS-E)

National University of Sciences and Technology (NUST)

H-12, Islamabad 44000, Pakistan

August 2022

Thesis Acceptance Certificate

Certified that final copy of MS/MPhil thesis written by **Mr. Tahir Javed** (Registration No. **00000277727**), of **USPCAS-E** has been vetted by undersigned, found complete in all respects as per NUST Statues/Regulations, is within the similarity indices limit, and is accepted as partial fulfillment for the award of MS/MPhil degree. It is further certified that necessary amendments as pointed out by GEC members of the scholar have also been incorporated in the said thesis.

Signature: _____

Name of Supervisor: **Dr. Majid Ali**

Date: _____

Signature (HoD): _____

Date: _____

Signature (Dean/Principal): _____

Date: _____

Certificate

This is to certify that work in this thesis has been carried out by **Mr. Tahir Javed** and completed under my supervision in **Thermal Energy Laboratory**, US-Pakistan Center for Advanced Studies in Energy (USPCAS-E), National University of Sciences and Technology, H-12, Islamabad, Pakistan.

Supervisor: _____

Dr. Majid Ali
USPCAS-E
NUST, Islamabad

Co-Supervisor: _____

Dr. M. Israr Siddiqui
NICE
NUST, Islamabad

GEC member 1: _____

Dr. Muhammad Bilal Sajid
USPCAS-E
NUST, Islamabad

GEC member 2: _____

Dr. Mariam Mahmood
USPCAS-E
NUST, Islamabad

GEC member 3: _____

Dr. Mustafa Anwar
USPCAS-E
NUST, Islamabad

HOD TEE: _____

Dr. Majid Ali
USPCAS-E
NUST, Islamabad

Principal: _____

Prof. Dr. Adeel Waqas Ahmad
USPCAS-E
NUST, Islamabad

Dedication

I would like to wholeheartedly dedicate this thesis to my beloved parents who supported me financially, spiritually, and emotionally throughout my life. Without their kind-heartedness and belief in me, I would not have been able to achieve this milestone.

To my siblings, mentors, and friends who shared their words of advice and encouragement to help me finish this study.

Abstract

The swirl flow generates when an axial flow stream gets a tangential component of velocity, which creates irregular maneuvering of flow particles. This random and chaotic movement of particles in swirl flow causes well mixing of fluid even at a homogeneous level, efficient heat conduction, and also helps us in separation through the centrifugal process. These important factors motivated us to understand and study swirl flow in a different restrictive manner by framing an experimental setup. In this study, the experimental investigation of swirl flow in a vertical transparent cylinder was carried out to examine the effect of the ribbed wall on the flow dynamics. The instantaneous velocity was obtained and the flow parameters were studied using the flow visualization technique Particle Image Velocimetry (PIV). The effect of ribs on turbulence was studied for velocity, vorticity, and swirl strength. The shape of square and semi-circular ribs was selected for this study and installed at equal distances quarterly inside the cylinders. The studies were performed at different RPMs 300, 400, and 500, and revealed the impact of RPMs on mixing and turbulence. Results revealed that the mixing was improved by using semi-circular ribs compared to square ribs and plain cases. The increase in RPM also agitated particles more chaotically and this turbulent behavior improved mixing.

Keywords: Swirl Flow; PIV; Mixing; Vorticity; Ribbed Cylinders.

Table of Contents

List of Figures

List of Tables

List of Publications

Conference: 6th International conference on **Energy, Environment, and Sustainable Development 2022 (EESD 2022).**

Title: Experimental study of swirl flow in a cylindrical container using Particle Image Velocimetry.

Authors: Tahir Javed, M. Israr Siddiqui, Majid Ali.

Accepted: December 06, 2021

Presented: January 18, 2022.

Nomenclature

Nomenclature

H	Height of laser, mm
k–ε	k-epsilon turbulence model
k–ω	k-omega turbulence model
r	Distance from the center (radius), m
Re	Reynolds number
u	x-component of velocity
v	Velocity of fluid, ms^{-1}
v_{avg}	Average velocity of fluid, ms^{-1}
v	y-component of velocity
v_r	Radial velocity
v_θ	Tangential velocity, ms^{-1}
v_z	Axial velocity
w	z-component of velocity

Greek Symbols

ρ	Density of the fluid, kgm^{-3}
μ	Dynamic viscosity of the fluid, Pa.s
μs	Microsecond
μm	Micrometer
ω	Angular velocity, $rads^{-1}$

List of Abbreviations

CAD	Computer Aided Design
CFD	Computational Fluid Dynamics
DES	Detached Eddy Simulation
DNS	Direct Numerical Simulation
FFT	Fast Fourier Transform
GLCC	Gas-Liquid Cyclone Separator
HGS	Hollow Glass Spheres
HPIV	Holographic Particle Image Velocimetry
IA	Interrogation Area
MRF	Multi Reference Frame
MSF	Measure Scale Factor
PC	Personal Computer
PIV	Particle Image Velocimetry
RNG	Re-Normalization Group
RPM	Revolutions Per Minute
SPIV	Stereoscopic Particle Image Velocimetry
SST	Shear Stress Transport
TPIV	Tomographic Particle Image Velocimetry
USLF	Upper Swirling Liquid Film
μPIV	Micro Particle Image Velocimetry

Chapter 1 : Introduction

1.1 Swirl Flow

When the tangential component of velocity is given to the axial flow, it produces a rotational force that disturbs the surface tension and equilibrium of flow. This is known as the swirl flow. One can see chaotic streamlines enveloping each other till it gets zero radii, which form vortices and eddies as well. Figure 1.1 shows a particle in a swirl motion.

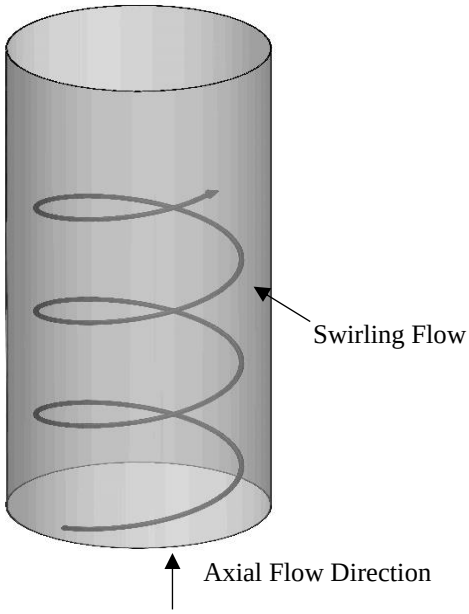

Figure 1.1: A particle in a swirl motion

Important parameters on which swirl flow depend are maximum tangential velocity and axial velocity of flow which help us to find the degree of swirl flow [1].

Both natural and forced kinds of swirl flows have distinct importance in human life in engineering, industries, and sciences. Understanding swirl flows are the complex part where analytical methods do not respond well due to their turbulent behavior. That's why we mostly use numerical simulations or experimental methods like Particle Image Velocimetry (PIV).

Numerical simulations have limitations like the modeling of mathematical models, discretization of domains, and numerical iterative simulation cost, which make them less attractive than experimental analysis.

Particle Image Velocimetry is providing the best system by adding seeding particles to the defined experimental flow to capture images by camera. Seeding particles have

a density equal to that of the fluid used and their size should be appropriate so that they make less effect on flow and provide the best visibility to the camera.

Due to its numerous technical and industrial applications, swirl flow research is extremely important. Where we need mixing, we need swirls. Mixing mostly plays its roles in fields like food processing industries, mining industry, HVAC systems, aviation industry for combustion, energy generation systems, etc [2]–[7].

The most important ones are briefly discussed below.

1.2 Applications of Swirl Flow

1.2.1 Cyclone Separator

A cyclone separator is used to separate particles from gases and liquids. It works when we force a flow to a conical-shaped container which makes a swirling kind of flow. It is where the use of a swirl becomes important and separates particles from gases and liquids. Swirl flow allows separation and well-mixed showering of particles to easily separate from other ones. Figure 1.2 represents the swirl flow in a cyclone separator.

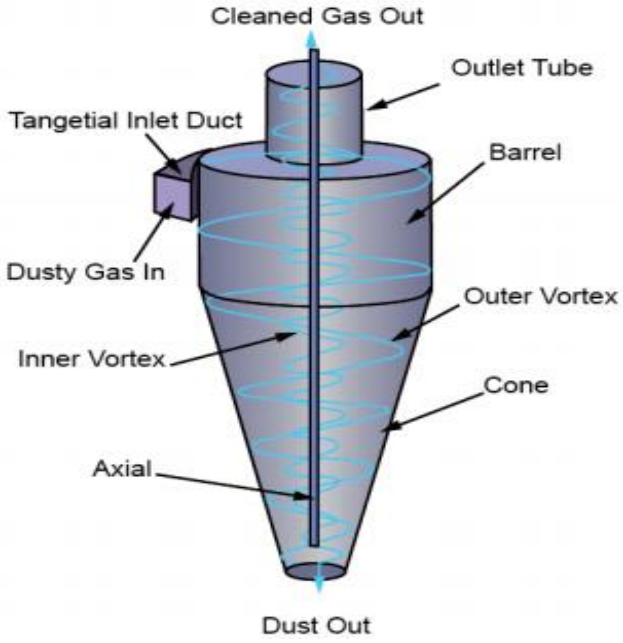

Figure 1.2: Swirl flow in cyclone separator [8]

1.2.2 Heat Exchanger

A heat exchanger transfers thermal energy from one fluid to another. Equal distribution of flow around tubes of the heat exchanger is important for equal absorption of heat. Swirl flow can perform this task by forcing the fluid particles to maneuver around the heat exchanger tubes and making this process effective and efficient, and improving the cost-effectiveness of the overall system (Figure 1.3).

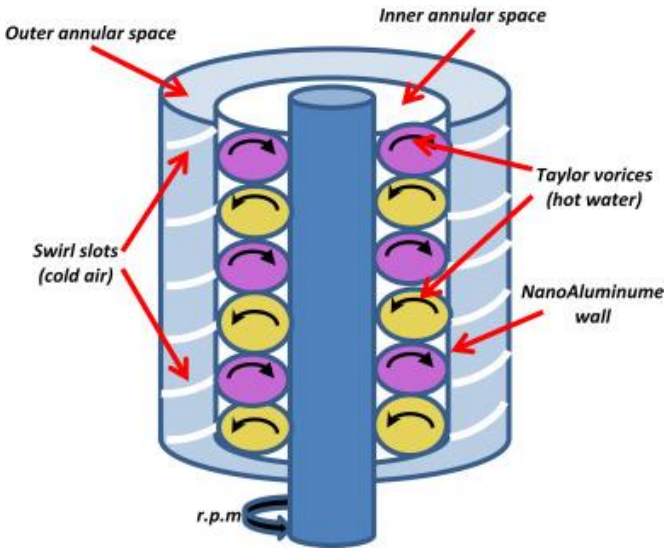

Figure 1.3: Swirl flow in heat exchanger [9]

1.2.3 Gas Turbines

A gas turbine is an integral part of the energy generation system to light our homes and run our economy. In gas turbines, the main principle is where the air comes with high pressure and face sprinkling of fuel gas on it to make a blast which forces turbine blades to run and rotate stator to generate electricity. When air comes and interacts with the gas fuel, it requires well mixing to generate a strong blast to propel a propeller. Swirl flow can easily do this job by just shaping airways into certain directions and will provide well mixing (Figure 1.4).

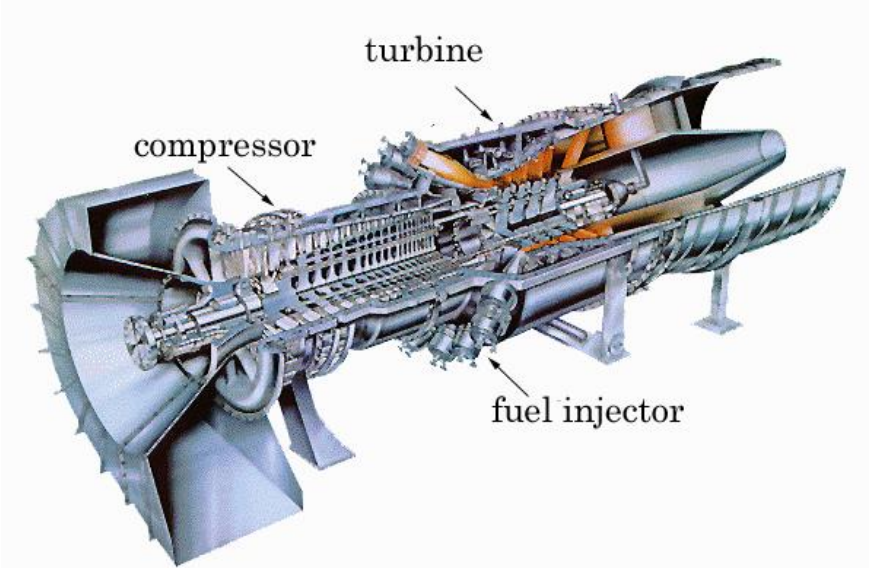

Figure 1.4: Swirl flow in gas turbine [10]

1.2.4 Pollution Control Devices

Pollution has enveloped the whole globe and the consequences are drastic. In pollution control devices, air passes through filters and unwanted particles stick to the filter surface and just allow the passing of clean air. When air passes through filters, it requires complete sprinkling and equal distribution to make it effective. By providing swirl air, it can be done easily (Figure 1.5).

Figure 1.5: Swirl flow in pollution control devices [11]

1.2.5 Food industry

The food industry also requires the mixing of different pastes and fluids homogeneously where the containers are rotated in the clockwise and anticlockwise directions and generate swirls and vortices for better mixing (Figure 1.6).

Figure 1.6: Swirl flow in the food industry [12]

1.3 Types of Swirl Flow

1.3.1 Free vortex flow

When the behavior of flow creates vortices by its internal changes in the particle movement, not by the external energy, it is known as free vortex flow. Examples:
Flow through kitchen sink, a whirlpool in a river, house rainwater drainage system, and tornadoes flow behavior.
The product of tangential velocity (v) and the distance from the center (r) is a constant (equation 1.1).

$$vr = \text{constant} \quad \ldots\ldots\ldots\ldots\ldots\ldots\ldots\ldots (1.1)$$

1.3.2 Forced Vortex flow

When we stir flow by forces and this agitation can be by pump, rotating base, or by providing base propeller like in washing machine. This is known as forced vortex flow. It is used mostly in applied sciences to improve the mixing and separation process.
The tangential velocity (v) is directly proportional to the radius (r) (equation 1.2).

$$v = r\omega \quad \ldots\ldots\ldots\ldots\ldots\ldots\ldots\ldots\ldots\ldots (1.2)$$

1.4 Swirl Generation Techniques

There are several ways to generate the rotation of a flow. Mainly we can generate swirls by using free and forced methods in any application. In the forced method, we give external energy to produce swirls and in free methods, diversions and hindrances can do likewise job to generate vortex and swirls. We divide swirl generation techniques into two classifications:

1.4.1 Power Generated

- Use of propellers that tangentially deflect the axial flow in any container [13]
- Rotation of container
- Using a stirring mechanism that generates a rotational movement to the fluid passing between them

1.4.2 Hindrances Generated

- By providing diversions to the flow
- By making a special shape of pipe or tube for fluid to flow in pipe or tube

1.5 Flow Velocity Measurement Techniques

There are different flow velocity measurement techniques. They are intrusive and non-intrusive measuring techniques. Intrusive measuring techniques include Pitot-Static Probe, hot wire, hot film, etc. In non-intrusive techniques, there are particle-based techniques and molecule-based techniques. Particle-based techniques are Laser Doppler Velocimetry (LDV), Planar Doppler Velocimetry (PDV), and Particle Image Velocimetry (PIV). Molecular-based techniques are Laser Induced Fluorescence (LIF) and Molecular Tagging Velocimetry (MTV). In this study, the Particle Image Velocimetry technique has been used. Figure 1.7 demonstrates a flowchart diagram of flow velocity measurement techniques.

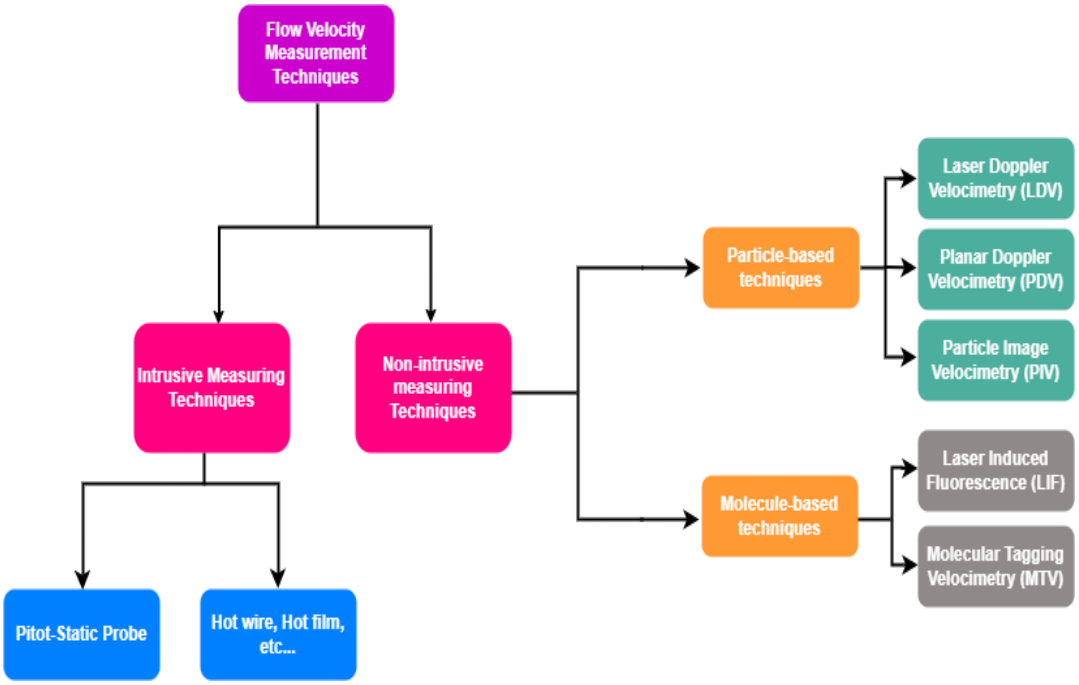

Figure 1.7: A flowchart diagram of different flow velocity measurement techniques

1.6 Problem Statement

When an axial flow is given a tangential component of velocity, swirl flow is produced. Swirl flow has various applications in different industries such as mixing and transportation processes. Since the swirl flow has significant importance in fluid dynamics, numerous experimental, computational, and analytical research have been conducted on it. The effect of ribs on turbulence has not been studied in any depth. Instantaneous velocity field measurements are necessary for this type of research. A popular non-invasive experimental method that provides the whole velocity field of the flow instantaneously is known as Particle Image velocimetry (PIV).

1.7 Research Objectives

Following are the main objectives of this study, which are based on the problem statement:

1. To obtain entire instantaneous velocity fields of turbulent swirl flow in cylinders.
2. To study the effect of ribs on turbulence.
3. To study the factors which affect the mixing phenomenon.

1.8 Scope

The scope of this research project closely resembles its specified objectives. For the optical measurements, a unique experimental approach called Particle Image Velocimetry (PIV) was used. Instantaneous velocity data were obtained for the turbulent swirl flow. The experimental tests were conducted in transparent glass cylinders and water was used as the working fluid since it has almost ideal flow characteristics.

1.9 Thesis Outline

The thesis is divided into six chapters.

Chapter 1 focuses on the importance of using an experimental method to study swirl flow. It provides a comprehensive explanation of the significance and industrial applicability of the research subject. This chapter also includes the objectives and scope of the project.

Chapter 2 will provide a thorough literature review of swirl flow research. It will give an overview of the experimental and numerical studies conducted in the past to comprehend the behavior and dynamics of swirl flow. This chapter will also state the research gap that exists.

Chapter 3 will describe the 3D modeling of the test section, test section fabrication, PIV components, and experimental setup. This chapter will also discuss the experimentation process.

Chapter 4 will discuss a basic working principle of Particle Image Velocimetry and its procedures involved. The working of PIV is discussed in detail. Pre-processing and post-processing will be explained in this chapter.

Chapter 5 will present results obtained after experimentation and the discussion. A detailed description of the results of the swirl flow system will be discussed.

Chapter 6 will cover conclusions keeping in view the results of the experiments. Furthermore, the recommendations are also discussed.

Summary

The importance of swirl flow and its applications have been explained in the starting section of this chapter. A brief overview of the problem statement is discussed in this chapter. The next section includes the objective of this research work. Furthermore, the scope of the research project has been explained.

References

[1] N. Gui, S. Jiang, J. Tu, and X. Yang, “Application in gas-particle flows,” in Gas-Particle and Granular Flow Systems, vol. 4, Elsevier, 2020.

[2] M. J. Doby, A. F. Nowakowski, E. Nowak, and T. Dyakowski, “Numerical and experimental examination of swirl flow in a cylindrical container with rotating lids,” Miner. Eng., vol. 20, no. 4, pp. 361–367, 2007.

[3] W. Liu, S. Jiang, and H. Li, “Experimental study of liquid-carrying by swirling flow in a U-shaped tube,” Exp. Therm. Fluid Sci., vol. 130, no. June 2021, p. 110479, 2022.

[4] Y. Zhao and R. Weber, “Combustion Accelerated Swirling Flows in High Confinements,” Prog. Energy Combust. Sci., vol. 78, pp. 349–367, 1992.

[5] A. D. Rocha, A. C. Bannwart, and M. M. Ganzarolli, “Numerical and experimental study of an axially induced swirling pipe flow,” Int. J. Heat Fluid Flow, vol. 53, pp. 81–90, 2015.

[6] Y. Rao, C. Biegger, and B. Weigand, “Heat transfer and pressure loss in swirl tubes with one and multiple tangential jets pertinent to gas turbine internal cooling,” Int. J. Heat Mass Transf., vol. 106, pp. 1356–1367, 2017.

[7] M. Sheikholeslami, M. Gorji-Bandpy, and D. D. Ganji, “Review of heat transfer enhancement methods: Focus on passive methods using swirl flow devices,” Renew. Sustain. Energy Rev., vol. 49, pp. 444–469, 2015.

[8] S. S. P. and A. R. N. Prachi K. Ithape, S. B. Barve, “Effect of Geometric Parameters on the Performance of Cyclone Separator,” Int. J. Curr. Eng. Technol., vol. m, no. 7, pp. 288–292, 2017.

[9] W. M. Hashim, H. A. Hoshi, and H. A. Al-Salihi, “Enhancement the performance of swirl heat exchanger by using vortices and NanoAluminume,” Heliyon, vol. 5, no. 8, p. e02268, 2019.

[10] “About gas trubine engine structure and torque.” http://turbotrain.net/en/whatsgasturbine.htm (accessed Nov. 07, 2021).

[11] “Dust Collection System for Foundry, Steel, Sponge Iron - Techflow.” https://techflow.net/foundry.html (accessed Nov. 07, 2021).

[12] “Food Technology - Framo Morat - Your idea - Our drive.” https://framo-morat.com/industries/food-technology/ (accessed Nov. 07, 2021).

[13] C. O. Iyogun, M. Birouk, and J. A. Kozinski, “Experimental investigation of the effect of fuel nozzle geometry on the stability of a swirling non-premixed methane flame,” Fuel, vol. 90, no. 4, pp. 1416–1423, 2011.

Chapter 2 : Literature Review

To move forward in research, we need to understand first what has been done in the recent past and how one can connect points to make a clear picture. In the scope of research, PIV is an important technique to get the confidence to use it in the study of swirl flow, so it is discussed thoroughly. Swirl flow effect on mixing and its dependence upon hindrances need to be studied. That's why in this chapter, the literature review has been discussed thoroughly. A brief review of the available PIV techniques has been done in the starting section of this chapter. The swirl flow effect in various shaped containers has been discussed in the next section. Furthermore, various hindrances' effect on swirl flow has been explained in detail. Different PIV techniques are described below.

2.1 PIV Techniques

2.1.1 2D2C PIV

The in-plane velocity components are measured using the two-dimensional, two-component (2D2C) PIV setup. Particle displacements in the object plane are used to determine the velocity field in 2D2C systems, which require only one camera. A light sheet illuminating the tracer particles that are moving with the flow defines the plane (2D). In 2D2C PIV, the illuminated region is captured on two consecutive image frames of a high-resolution camera [1], [2].

2.1.2 Stereoscopic PIV

This is also known as 3-component (3C) PIV. The z-axis displacement is extracted using two cameras with different viewing angles in stereoscopic PIV. To define displacement in the x, y, and z-axes within a unit of time, the variables *u*, *v*, and *w* are frequently used in fundamental fluid mechanics. The in-plane x and y directions are used in basic PIV to obtain *u* and *v* displacements. This makes it possible to calculate the x and y gradients. However, the other 5 terms of the velocity gradient tensor cannot be determined using this information.

The stereoscopic PIV analysis also provides the z-axis displacement component, *w*, within the same plane. This gives two additional velocity gradient terms, x, and y, in addition to the z-axis velocity of the fluid at the plane of interest. It is not possible to calculate the components of the velocity gradient x, y, and z.

The three components of velocity vectors in the laser-illuminated region can be measured simultaneously using the Stereo PIV technique, which is considered to be the simplest technique to use. Two cameras are used to capture the stereoscopic images, either with an offset distance or at different viewing axes. Stereo PIV calculations can produce an in-plane spatial resolution that is significantly higher than that of tomographic PIV and 3D Particle Tracking Velocimetry (PTV) techniques. Regarding the measuring plane, thousands of flow velocity vector fields can be provided [3].

2.1.3 Holographic PIV

The whole three-dimensional representation of flow velocity fields can be captured using holographic PIV technologies. By using holography to capture the image, holographic PIV can determine all 3 components related to velocity vectors over the whole volume of fluid flow [4]. The best measurement precision and spatial resolution are provided by HPIV when compared to other PIV methods currently in use [5].

But HPIV is also considered one of the more complicated PIV methods. The development of the latest data processing methods is required for HPIV, along with significant investments in optical alignments and equipment. To effectively use HPIV as a PIV method for various complicated engineering fields, much work is still required [6].

The low dispersion performance of particles, the poor depth resolutions, and instabilities in the restructuring has been effectively solved by the development of advanced equipment. Additionally, effective methods are presented to examine the holographic memory and process a large amount of data to provide a final flow field approximation [7]. In general, holography is a technique for storing the amplitudes and phase of a light beam by capturing the interference arrangement created when a second wave, referred to as the reference wave, is overlapped [8].

By lighting the produced interference arrangement with a duplicate of the reference wave, the original wave pattern can be recreated as a hologram [9]**.** There are various approaches for performing particle capturing.

2.1.4 Tomographic PIV

Tomographic PIV uses multiple cameras at various viewing angles for simultaneously observing a volume to obtain details about its depth.

The modern three-component, three-dimensional velocity measuring technique is known as Tomographic Particle Image Velocimetry. This technique allows the volumetric lighting of a tracer-particle region while simultaneously imaging it from various perspectives, whereas synchronous particle images are used for tomographic reformation to estimate the three-dimensional Mie-scattering region. The resulting tomogram sets are divided into interrogation areas, and the cross-correlation projection of the average particle movement is performed. Therefore, fluid velocity fields can thus be quickly measured thanks to TPIV [10].

Without the requirement to identify the distinct particles, the tomographic-PIV analysis approach can resolve the motion of particles inside a three-dimensional measuring volume. This most recent technique relies on multiple digital cameras placed in different viewing orientations, simultaneously observing the illuminated particles.

2.1.5 Micro PIV

There are several fields of research and technology where understanding the flow pattern at the micron size is important. Aviation, computing, automobile, and biomedical sectors all use micro-fabricated fluidic systems in productive ways.

For a wide range of purposes, this measuring technique is similar to Particle Image Velocimetry. The visual method quantifies two-component velocity distribution in a two-dimensional measuring plane using typical microscopy and digital photographic techniques. Clear working media and visual access to areas of interest are required for the optical measuring approach. To visualize the displacement of fluid, tracer particles are dispersed into the flow. A microscopic object is used to light and examine a volume of fluid containing tracer particles. A standard installation of a micro PIV for collecting data comprises a laser light that is timed to synchronize the digital camera. A typical continuous wave light origin for PIV is frequency-doubled Nd: YAG laser beams with a wavelength of 532 nm. Micro PIV applications require less than 10mJ of laser power per pulse [11].

2.2 Swirl Flow in Various Shaped Containers

Liu et al. [12] performed a visualization experiment to investigate the capability of a swirl flow in a U-shaped conduit to carry liquid as shown in Figure 2.1. Using the signals from the fluctuation of the liquid film height, they also studied the process underlying the enhanced swirl flow capability. Furthermore, they determined the

liquid-carrying operation range of the swirling flow. Both the liquid-carrying capacity and the gas-liquid interface fluctuation increased as the gas flow rate did.

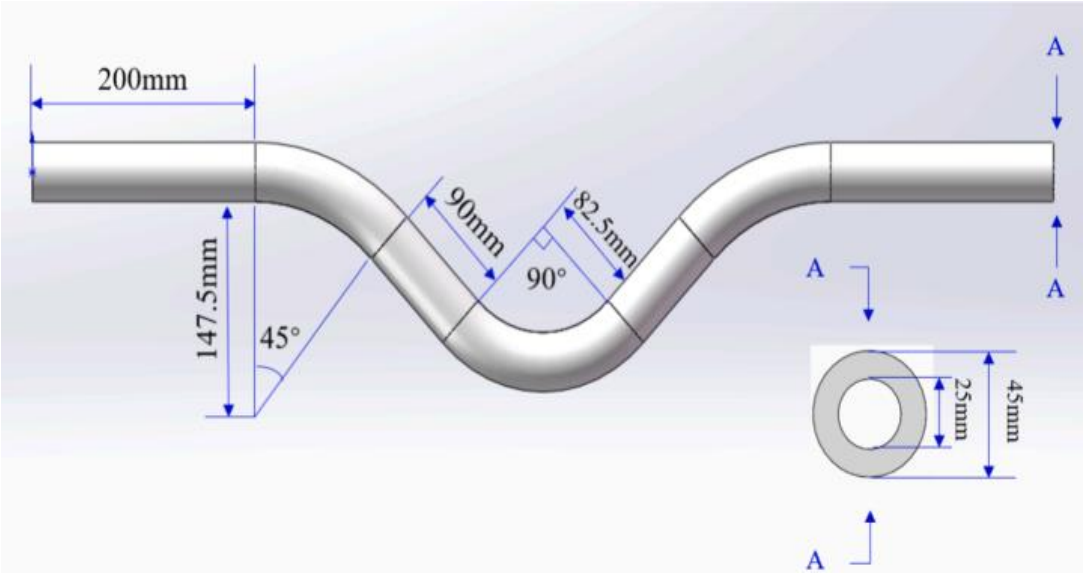

Figure 2.1: The geometric details of U-shaped tube [12]

Ichiyanagi et al. [13] experimentally determined the in-cylinder swirl flow velocities in a single-cylinder diesel engine at different driving conditions using PIV. They analyzed the intake and compression strokes using the flow velocities during various driving conditions. While comparing the maximum velocity at various engine speeds, they also observed that the flow pattern fairly remained unchanged, but the flow velocity increased with the increase in engine speed. The core of the swirl changed at each crank angle followed by a counter-clockwise path and varied at each plane. Moreover, while evaluating the swirl ratio at various helical port opening ratios, there was an increase in the swirl ratio with a decrease in the opening ratio.

Ivan Božić [14] used a modern method to calculate elbow draft tube inefficiencies for the essential broad range on-cam operation modes of the Kaplan turbine as illustrated in Figure 2.2. The research aimed at how swirl flow characteristics, which were set for the corresponding inflow of the draft tube, affected hydraulic losses. A novel formula for calculating draft tube losses was given based on the methodology and numerical results obtained.

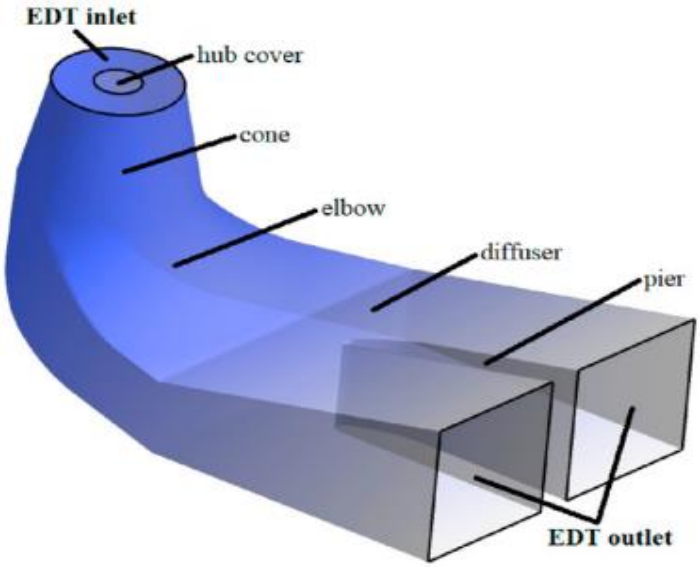

Figure 2.2: Elbow draft tube of a Kaplan turbine [14]

To investigate the thermal performance in a single tube with the simulated swirl separator (Figure 2.3), Abe et al. [15] employed a RANS (Reynolds-averaged Navier-Stokes equations) computation using three isotropic modeling techniques: standard *k*–*ε*, realizable *k*– *ε*, and SST *k*–*ω* models. Their findings showed that the calculated wall surface temperature and heat transfer coefficient (HTC) resulting from the SST *k*–*ω* model was generally consistent with the experimental data. Their findings suggested that while evaluating HTC augmentation downstream of the spacer, it was critical to look at turbulence formation.

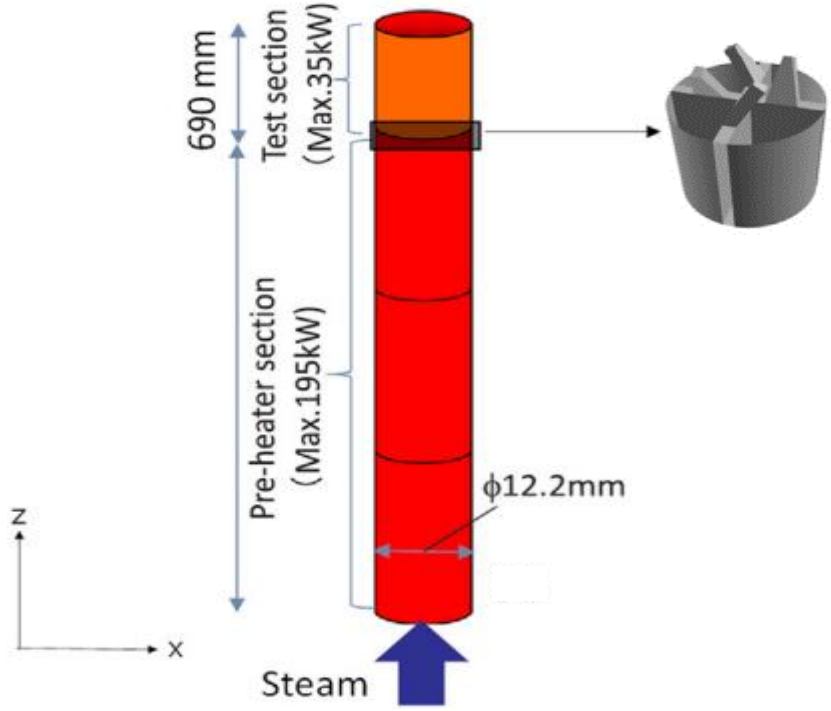

Figure 2.3: A single-tube test apparatus and swirl spacer [15]

Shafee et al. [16] used a helical turbulator to improve the convective flow within a pipe. For nanomaterial modeling, a homogeneous model was used. The ranges of the Reynolds number (Re) and turbulator width (b), respectively, were 5000 to 15000 and 5 to 15mm. A pure carrier fluid was added to copper oxide nano-particles to improve thermal behavior. Their results revealed that when the turbulator width was increased, the mixing of the boundary surface and the inner nano-fluid flow became more effective.

To test if the energy equation, which includes the considerable derivative of pressure and the viscous dissipating terms, could accurately compute the energy conversions from kinetic to thermal energy in an irreversible process, Yusof et al. [17] numerically solved it. The fluid temperature was determined for a swirl flow in a cylinder with a fixed initial angular velocity as shown in Figure 2.4. The temperature of the fluid increased as a result of the kinetic energy of the fluid transformed into thermal energy. The results revealed that a rate of 99.4 percent was used to transform the original state of kinetic energy into thermal energy.

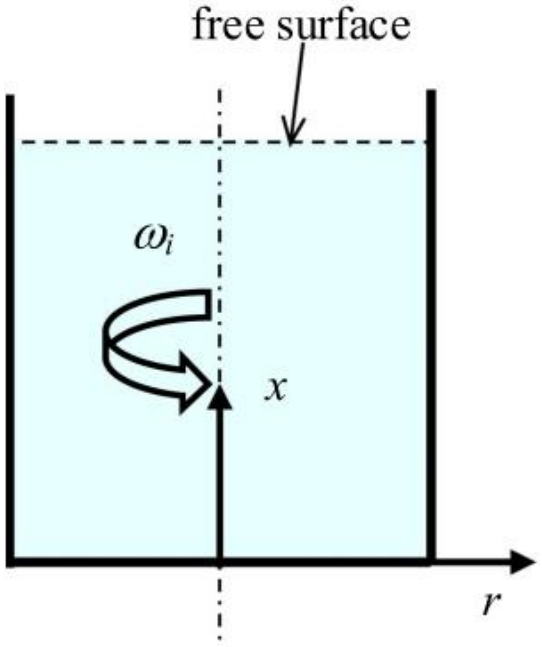

Figure 2.4: Swirling flow in a cylinder with angular velocity ω_i [17]

Xu et al. [18] used the 2D PIV technique to study swirl flow dynamics in a water conical pipe exposed to a repeated oscillating wall at a Reynolds number of 3800. They studied various parameters like flow velocity, instantaneous axial and vertical velocity, mean velocities, and Reynolds stresses. Their findings demonstrated the formation of

a transitional recirculation cell in the center of the pipe. They further revealed how vibration significantly reduced the variation in velocity while enhancing the uniformity of the swirl flow.

Hreiz et al. [19] used the flow visualization technique to characterize the swirling flow in the gas-liquid phase for a gas-liquid cylindrical cyclone separator (GLCC) (Figure 2.5). The vortex core could be visualized thanks to bubbles in the vortex acting as a tracer. Their findings demonstrated that the bubbly filament had extremely complicated hydrodynamics, with a transition through laminar and turbulent regions. Near the vortex center, the laminar region was related to downward velocities. Upward velocities towards the vortex center were caused by turbulent puffs and an unfavorable pressure gradient in the vortex center. Finally, based on their findings, they proposed that numerous tangential inlets could be used in GLCCs to enhance separation efficiency.

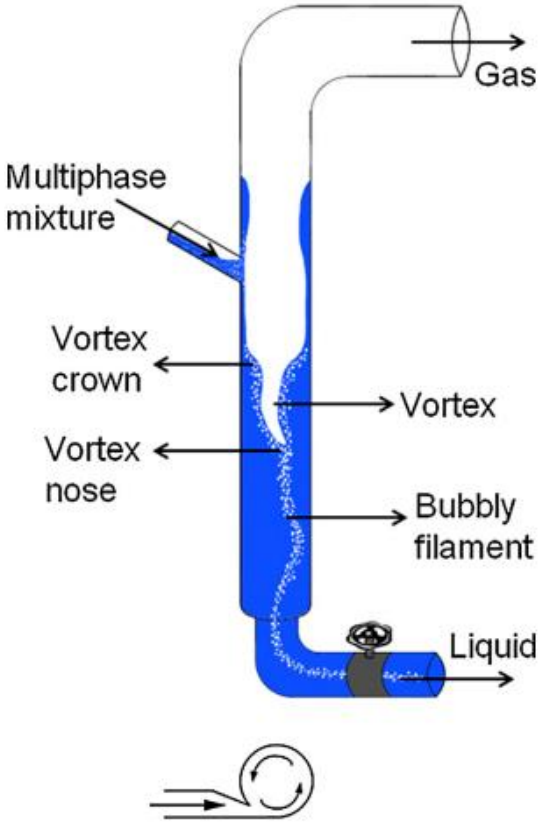

Figure 2.5: Schematic diagram of the GLCC and the nozzle [19]

Doby et al. [20] applied different experimental and numerical techniques to study swirl flow. They used an optically transparent cylinder having revolving lids to investigate the fundamental mechanics of swirling in the laminar region. Their findings were the

first step in a series of tests aimed at improving the separation mechanism of hydro-cyclones by controlling swirling flow parameters.

Chang et al. [21] experimentally studied the time-averaged velocity profiles with and without swirl flow using the PIV technique. They also experimentally studied the properties of turbulent behavior of water flow in a horizontal circular tube employing the liquid crystal. Their findings agreed well with that of the literature.

Caldeira et al. [22] experimentally investigated the flow field at the output/outlet of a mixing container of a Lean Premixed Prevaporized Combustor (LPP) using the PIV technique. Their combustor design consisted of a single swirler that had several movable vanes that allowed the swirl number to be adjusted. They found that there was a significant amount of flow recirculation inside the combustion chamber, based on the swirl number. The velocity fields showed different regimes with the variations in the swirl number.

2.3 Hindrances Effect on Swirl Flow

W. Wodziak et al. [23] experimentally studied the turbulent behavior of the flow of air in a channel having one ribbed wall using PIV. They used equally spaced trapezoidal ribs (Figure 2.6) to study the turbulent flow. The region where the transition of the airflow structure from the d-type flow to the k-type flow occurred had a ratio of the width between the consecutive ribs to the rib height (w/k) of five. The observations were made at an input velocity where the Re was 32,500. Their results revealed that two vortices with the same rotational direction were developed in the recirculation region among the ribs. The flow patterns that were seen agreed with the transitional region of literature descriptions.

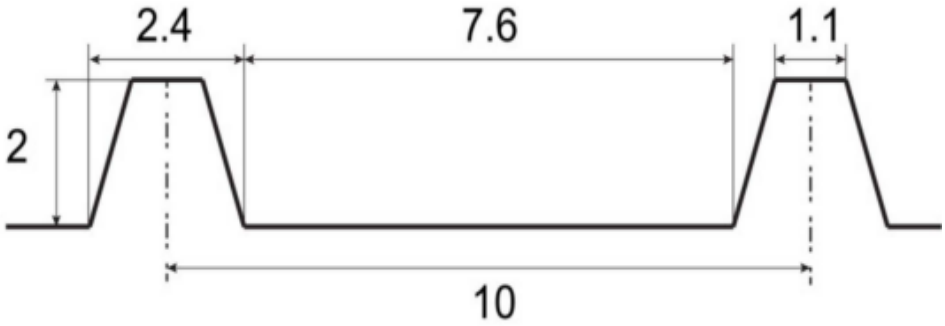

Figure 2.6: Shape of trapezoidal ribs (dimensions in mm) [23]

Following the observation and identification of the flow structures of the upper swirling liquid film (USLF) and experimental measurements of its thickness and pressure, Y. A. Wang et al. [24] calculated the swirl frictional factors of the Gas-Liquid Cylindrical Cyclone (GLCC). The flow pattern criteria were eventually developed. Their findings revealed that the liquid layer did not significantly vary in thickness around the circumference after leaving the inlet. Using measurements of the liquid layer thickness and pressure loss, the GLCC friction factors were calculated.

H. Li et al. [25] examined the overall effect of rotating continuous ribs on turbulent flows and flow separation caused by square duct construction. The rotation number varied from 0 to 0.52, and a constant Reynolds number of 10,000 was used. They employed a time-resolved particle image velocimetry technique to describe the fundamental flow and turbulence dynamics. Their results revealed that the rotation considerably altered the features of the primary flow and turbulent flow dynamics. A significant flow behavior was specifically observed in that due to flow separation along the ribs, the velocity distribution shifted to the front side. Moreover, the velocity distribution pattern shifted to the following side once the rotation number reached 0.48 (critical value).

Foukrach et al. [26] investigated how different types of agitators affected turbulent flows in stirred tanks with and without baffles. The hydrodynamic behavior caused by four different agitators was numerically predicted using the Navier-Stokes equations and the RNG–turbulent model. The Multi Reference Frame (MRF) method was used to run the simulations. The numerical results matched the experiment very well. They discovered that the agitator converging triangular blade turbine (CTBT) saved a significant amount of energy per ratio when compared to the others and that the agitator diverging triangular blade turbine (DTBT) reduced the vortex size of the impeller angles significantly.

Sharma et al. [27] carried out an experimental examination of comprehensive flow field observation in a rectangular channel with truncated prismatic ribs (Figure 2.7) installed on the bottom surface using two-dimensional particle image velocimetry (2-D PIV). They found that compared to square ribs, truncated prismatic ribs had a significantly smaller main recirculation bubble and a shorter reattachment length.

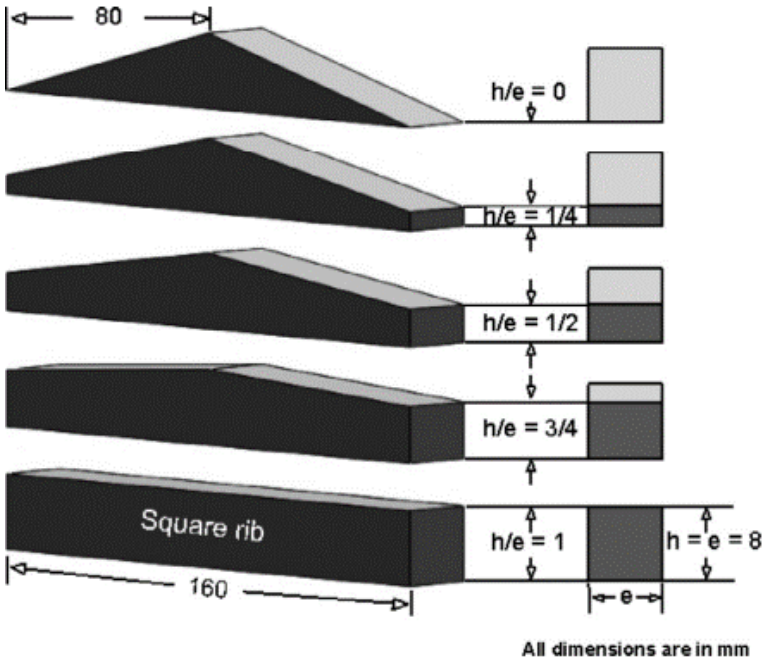

Figure 2.7: The geometry of truncated prismatic rib turbulators [27]

Chuangxin et al. [28] used different measuring techniques to examine the impacts of a near-wall square rib on flow pattern and surface heat transfer enhancement. The techniques included split-fiber film probing, planar particle image velocimetry, and temperature-sensitive paint (TSP). The flow characteristics in the wake of the rib were shown by combining velocity field calculations using PIV with complementing calculations by the split-fiber film when the G/d (Gap size to rib size ratio) was equal to 0.25. Near the surface, a very small separation bubble with very irregular flow reversal was observed.

Jansson et al. [29] investigated the inviscid linear stability of a solid cylindrical container enclosed by a constrained swirling flow with constant vorticity according to two-dimensional hindrances. By decomposing the problem using the superposition principle, they were able to show that the linear inviscid stability concerning rotating disturbances was not related to the boundary conditions. It was stated that a merged homogeneous state was the one in which the mass of the solid was equal to the mass of the displaced fluid and the flow was rotational like a rigid body.

Detached Eddy Simulation (DES) of cyclones cooling flow and the heat transfer in a swirling tube was studied by Biegger et al. [30] and compared to their experimental measurements. The numerical technique was justified using data from direct numerical simulation (DNS) research simulating a turbulent channel flow. There was good

agreement between the DES and the experiment in terms of mean velocity profiles and turbulent kinetic energy. The simulation somewhat underestimated the heat transfer coefficients near the intake, but they agreed further downstream.

Coletti et al. [31] conducted experiments having transverse ribs on one of the walls of a channel (Figure 2.8) in the turbulent flow region. The ribs used were about one-tenth the height of the channel, with a spacing of ten times their height. Based on the hydraulic diameter of the channel and the bulk flow velocity, the Reynolds number was 15,000. They used time-resolved particle image velocimetry to find velocity fields alongside the stream-wise plane. They found that although the separated flow was reattached before the next hindrance, there was a strong rib-to-rib contact. Span-wise vortices, measuring 0.2 rib heights, were developed in the free shear layer, moved over the pitch, and had an influence on the following rib.

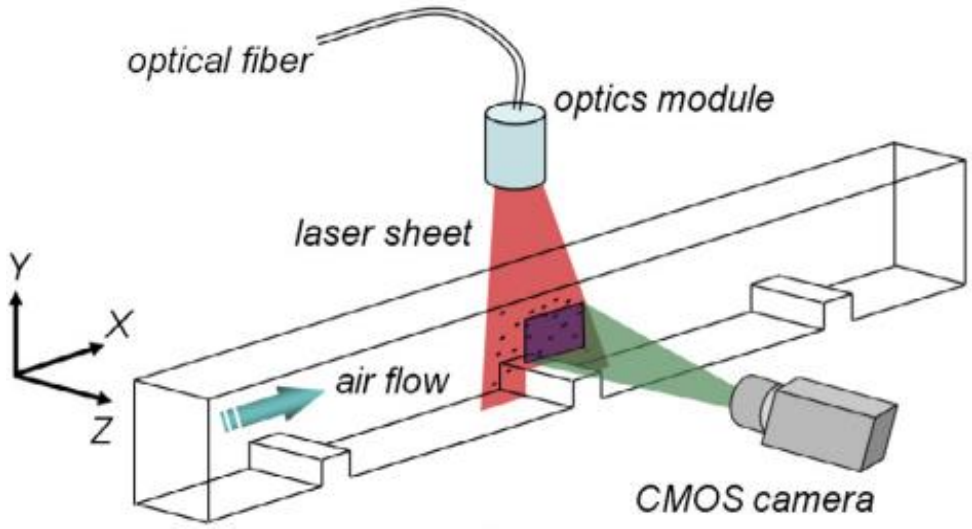

Figure 2.8: PIV measurements in a channel with transverse ribs [31]

Tsukahara et al. [32] investigated turbulent Taylor-vortex flows among two concentric cylindrical containers, and the interior cylinder was installed with the transverse ribs at fixed intervals. The internal cylindrical container, which had a radius of R_1, revolved at a constant angular velocity of ω whereas the external cylindrical container, which had a radius of R_2 as represented in Figure 2.9, remained fixed. They examined the influence of the ribs gap on the flow fields over the ribs and the flow resistances using parametric research and direct numerical simulation. Their most important finding was that with the increase in pressure (form) and drag caused by roughness was mitigated by the highly unfavorable pressure gradient behind all ribs that was aided by the in-flow motions of the Taylor vortices.

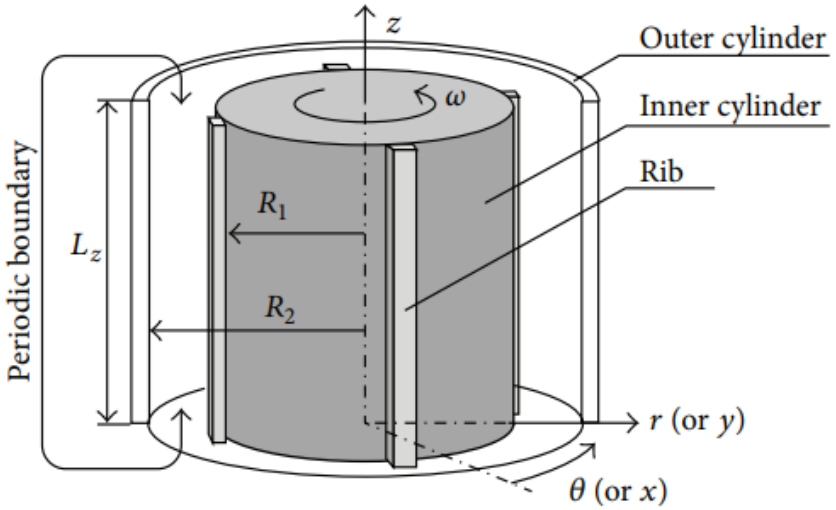

Figure 2.9: Geometry of ribbed inner cylinder [32]

V.P. Fragos et al. [33] employed the direct numerical simulation (DNS) method of transient Navier–Stokes and continuity equations applying Galerkin finite elements to examine the flow separation and reattachment of two-dimensional and turbulent flow around a rib. The simulation results were obtained and flow properties for six particular Reynolds numbers, ranging from 1304 to 2500, were discussed. Vortex shedding, flapping motion, as well as turbulence data were among the many features of turbulent flow that were presented and explored. They compared the numerical results of their study with the experimental and numerical data of the other researchers.

Lei et al. [34] examined the flow dynamics in a channel having solid and perforated ribs on one of the walls using PIV. The Reynolds number selected was 22,000. They studied the flow parameters like mean velocity, vorticity, streamlines, turbulence intensity, and Reynolds shear stress. They found that the ribs with perforation had considerably fewer recirculation bubbles downstream of the rib than those with solid ribs. In comparison to solid ribs, the length of reattachment following perforated ribs was approximately 45 percent shorter. Furthermore, the perforated rib case had a smaller pressure drop than a solid rib case because the Reynolds shear stresses surrounding the perforated ribs were considerably lower.

Jawarneh et al. [35] carried out a numerical analysis to determine the separation efficiency of a double-phase, highly swirl flow in a cylinder-shaped separator with dual vortex generators for a mixture containing oil in the main phase and sand of a particular diameter in the secondary phase. They used the mixture-granular multiphase and RNG k–ε turbulence models. The consistency among the experimental data and

the simulation findings of the RNG k–ε model was satisfactory. Furthermore, their study demonstrated to be beneficial in determining the internal flow structure of the main phase, resulting in particle phase separation.

Lei et al. [36] performed an experimental analysis of the flow patterns and turbulent characteristics related to flow separation in a square channel roughened with stream wise periodic ribs on one wall using PIV. The Reynolds number used was fixed at 22,000. The different parameters studied were the generation of turbulent kinetic energy and shear stress, as well as mean velocity, friction coefficient, vorticity thickness, Reynolds shear stress, and anisotropy parameter. The results revealed that the large-scale, unsteady vortex patterns were dominant in the separated shear layer.

Sahu et al. [37] investigated five different impeller designs and predicted the flow field created by these impellers. The experimental measurements and the calculated values of dimensionless radial velocity v_r and dimensionless axial velocity v_z were observed to be in good accordance. The dimensionless tangential velocity v_θ predictions indicated a mixed pattern. They found that the use of zonal modeling considerably improved the predictions of turbulent kinetic energy.

2.4 The Gap in Literature Review

In the literature review, I found a gap in academic research where there was a need to study the effect of ribs in the cylindrical container using Particle Image Velocimetry to understand the swirl flow behavior. In this research, swirl flow and mixing were investigated experimentally using PIV. Transparent glass cylinders were used for the experiments, which were conducted at 300, 400, and 500 revolutions per minute (RPM) for the plain, square ribs, and semi-circular ribs swirl flow cases.

Summary

This chapter includes a brief literature review of recent studies on swirl flow. The experimental and numerical research work of various researchers has been discussed. They used different experimental and numerical techniques for their work. The swirl flow behavior in various geometries used by different researchers has been discussed. The research works with different Reynolds numbers and the shapes of ribs have also been discussed. Finally, the general research being conducted about this work is explained in detail.

References

[1] F. G. Ergin, B. B. Watz, and N. F. Gade-Nielsen, “A review of planar PIV systems and image processing tools for lab-on-chip microfluidics,” Sensors (Switzerland), vol. 18, no. 9, pp. 1–23, 2018.

[2] “Planar PIV - Dantec Dynamics | Precision Measurement Systems & Sensors.” https://www.dantecdynamics.com/solutions-applications/solutions/fluid-mechanics/particle-image-velocimetry-piv/planar-piv-systems/ (accessed Nov. 21, 2021).

[3] H. Hu, “Stereo Particle Imaging Velocimetry Techniques: Technical Basis, System Setup, and Application,” Handb. 3D Mach. Vis. Opt. Metrol. Imaging, pp. 71–100, 2013.

[4] M. R. Abdulwahab, Y. H. Ali, F. J. Habeeb, A. A. Borhana, A. M. Abdelrhman, and S. M. Ali Al-Obaidi, “A review in particle image velocimetry techniques (developments and applications),” J. Adv. Res. Fluid Mech. Therm. Sci., vol. 65, no. 2, pp. 213–229, 2020.

[5] D. F. Hill, K. V Sharp, and R. J. Adrian, “The implementation of distortion compensated stereoscopic PIV,” Int. Work. PIV’99- St. Barbar. 3 rd, St. Barbar. CA, 1999.

[6] J. Katz and J. Sheng, “Applications of holography in fluid mechanics and particle dynamics,” Annu. Rev. Fluid Mech., vol. 42, pp. 531–555, 2010.

[7] M. Jahanmiri, “Particle Image Velocimetry: Fundamentals and Its Applications,” Fundam. Its Appl., pp. 1–58, 2011.

[8] P. J. Bryanston-Cross, M. Funes-Gallanzi, C. Quan, and T. R. Judge, “Holographic particle image velocimetry (HPIV),” Opt. Laser Technol., vol. 24, no. 5, pp. 251–256, 1992.

[9] R. J. Collier, C. B. Burckhardt, and L. H. Lin, Optical Holography. Academic Press, 1971.

[10] K. Kumashiro, A. M. Steinberg, and M. Yano, “High spatial resolution 3d fluid velocimetry by tomographic particle flow velocimetry,” AIAA Scitech 2019 Forum, no. January, pp. 1–11, 2019.

[11] R. Lindken, M. Rossi, S. Große, and J. Westerweel, “Micro-Particle Image Velocimetry (PIV): Recent developments, applications, and guidelines,” Lab Chip, vol. 9, no. 17, pp. 2551–2567, 2009.

[12] W. Liu, S. Jiang, and H. Li, “Experimental study of liquid-carrying by swirling flow in a U-shaped tube,” Exp. Therm. Fluid Sci., vol. 130, no. June 2021, p. 110479, 2022.

[13] M. ICHIYANAGI et al., “Effects of Intake Flow on In-Cylinder Swirl Flow Under Motoring and Firing Conditions for CI Engines using PIV Measurements,” J. Eng. Sci. Technol., vol. 16, no. 5, pp. 3600–3619, 2021.

[14] I. Božić, “A novel energy losses dependence on integral swirl flow parameters in an elbow draft tube of a Kaplan turbine,” Renew. Energy, vol. 175, pp. 550–558, 2021.

[15] S. Abe, Y. Okagaki, A. Satou, and Y. Sibamoto, “A numerical investigation on the heat transfer and turbulence production characteristics induced by a swirl spacer in a single-tube geometry under single-phase flow condition,” Ann. Nucl. Energy, vol. 159, p. 108321, 2021.

[16] A. Shafee et al., “Numerical simulation for turbulent flow in a tube with combined swirl flow device considering nanofluid exergy loss,” Phys. A Stat. Mech. its Appl., vol. 542, p. 122161, 2020.

[17] S. N. A. Yusof, Y. Asako, M. Faghri, L. K. Tan, N. A. B. C. Sidik, and W. M. A. B. A. Japar, “Energy equation of swirling flow in a cylindrical container,” Int. Commun. Heat Mass Transf., vol. 108, no. August, p. 104288, 2019.

[18] Y. Xu, Y. Y. Zhang, F. C. G. A. Nicolleau, and Z. C. Wang, “PIV of Swirling Flow in a Conical Pipe with Vibrating Wall,” Int. J. Appl. Mech., vol. 10, no. 2, 2018.

[19] R. Hreiz, C. Gentric, N. Midoux, R. Lainé, and D. Fünfschilling, “Hydrodynamics and velocity measurements in gas-liquid swirling flows in cylindrical cyclones,” Chem. Eng. Res. Des., vol. 92, no. 11, pp. 2231–2246, 2014.

[20] M. J. Doby, A. F. Nowakowski, E. Nowak, and T. Dyakowski, “Numerical and experimental examination of swirl flow in a cylindrical container with rotating

lids," Miner. Eng., vol. 20, no. 4, pp. 361–367, 2007.

[21] T.-H. Chang, D.-B. Nah, and S.-W. Kim, "Review of Experimental Studies on Swirling Flow in the Circular Tube using PIV Technique," Journal of the Korean Society of Visualization, vol. 7, no. 1. pp. 21–28, 2009.

[22] A. Caldeira-pires and R. Q. Neiva, "Swirling Flow Analysis using PIV," Procedings COBEM 2007, p. 7, 2007.

[23] W. Wodziak and J. Sobczyk, "PIV Measurements of Turbulent Airflow in a Channel with Trapezoidal Ribs on One Wall," Appl. Sci., vol. 12, no. 3, pp. 1–9, 2022.

[24] Y. A. Wang, J. Y. Chen, T. Yue, Y. Yang, M. S. Han, and C. Y. Yan, "Measurement of thickness and analysis on flow characteristics of upper swirling liquid film in gas-liquid cylindrical cyclone," Exp. Therm. Fluid Sci., vol. 123, no. February 2020, p. 110331, 2021.

[25] H. Li, H. You, R. You, and Z. Tao, "Experimental investigation of turbulent flow in a rotating straight channel with continuous ribs," Phys. Fluids, vol. 32, no. 1, 2020.

[26] M. Foukrach, M. Bouzit, H. Ameur, and Y. Kamla, "Effect of Agitator's Types on the Hydrodynamic Flow in an Agitated Tank," Chinese J. Mech. Eng. (English Ed., vol. 33, no. 1, 2020.

[27] N. Sharma, A. Tariq, and M. Mishra, "Experimental investigation of flow structure due to truncated prismatic rib turbulators using particle image velocimetry," Exp. Therm. Fluid Sci., vol. 91, no. November 2017, pp. 479–508, 2018.

[28] C. He, Y. Liu, D. Peng, and S. Yavuzkurt, "Measurement of flow structures and heat transfer behind a wall-proximity square rib using TSP, PIV and split-fiber film," Exp. Fluids, vol. 57, no. 11, pp. 1–18, 2016.

[29] I. Jansson and H. O. Åkerstedt, "The dynamics of cylinder in a confined swirling flow with constant vorticity," Eur. J. Mech. B/Fluids, vol. 54, pp. 98–104, 2015.

[30] C. Biegger, C. Sotgiu, and B. Weigand, "Numerical investigation of flow and heat transfer in a swirl tube," Int. J. Therm. Sci., vol. 96, pp. 319–330, 2015.

[31] F. Coletti, I. Cresci, and T. Arts, “Spatio-temporal analysis of the turbulent flow in a ribbed channel,” Int. J. Heat Fluid Flow, vol. 44, pp. 181–196, 2013.

[32] T. Tsukahara, M. Ishikawa, and Y. Kawaguchi, “DNS Study of the Turbulent Taylor-Vortex Flow on a Ribbed Inner Cylinder,” Adv. Mech. Eng., vol. 2013, 2013.

[33] V. P. Fragos, S. P. Psychoudaki, and N. A. Malamataris, “Two-dimensional numerical simulation of vortex shedding and flapping motion of turbulent flow around a rib,” Comput. Fluids, vol. 69, pp. 108–121, 2012.

[34] L. Wang, M. Salewski, and B. Sundén, “PIV Measurements of Turbulent Flow in a Channel with Solid or Perforated Ribs,” Am. Soc. Mech. Eng. Fluids Eng. Div. FEDSM, vol. 1, no. PARTS A, B AND C, pp. 1995–2003, 2010.

[35] A. M. Jawarneh, H. Tlilan, A. Al-Shyyab, and A. Ababneh, “Strongly swirling flows in a cylindrical separator,” Miner. Eng., vol. 21, no. 5, pp. 366–372, 2008.

[36] L. Wang, J. Hejcik, and B. Sunden, “PIV Measurement of Separated Flow in a Square Channel With Streamwise Periodic Ribs on One Wall,” J. Fluids Eng. Trans. ASME, vol. 129, no. 7, pp. 834–841, 2007.

[37] A. K. Sahu, P. Kumar, A. W. Patwardhan, and J. B. Joshi, “CFD modelling and mixing in stirred tanks,” Chem. Eng. Sci., vol. 54, no. 13–14, 1999.

Chapter 3 : Design, Fabrication, and Experimentation

As literature suggested that there was a gap to observe the swirl flow behavior in ribbed cylinders and their effect on mixing which compelled me to design an experimental setup by using the available system of Particle Image Velocimetry. The setup was first designed conceptually on paper to get the idea of the whole work where container size and shape were selected and shapes of ribs were also chosen. CAD modeling, test section fabrication, components of PIV, and experimental setup have been discussed in this chapter.

A series of experiments were carried out at different heights of a laser beam, first without rib configuration and then with square and semi-circular ribs. Experiments were carried out in cylinders at different RPMs of water like 300, 400, and 500 RPMs. A magnetic stirrer was used to give constant RPMs to water in the glass cylinder.

3.1 CAD Modeling of Test Section

As commercial softwares are providing opportunities to design Computer-Aided Design (CAD) models to get help in fabrication and assembly as well as show its attire how it will look like. The model of the section was made in the SOLIDWORKS software which is widely accepted in the mechanical community and provides a well-established system and tools to complete a model. This 3D model later helped me in the fabrication of the test section.

3.1.1 Transparent Cylindrical Container

A transparent cylindrical container was modeled with the help of software that was later fabricated and used in the experiment. Plain cylinder without ribs as well as ribbed cylinders having square and semi-circular ribs installed inside the cylinders were modeled. The dimensions of the cylinder are given in the following sections of this chapter. The 3D modeled glass cylinder is shown in Figure 3.1.

Figure 3.1: 3D modeled glass cylinder

3.1.2 Types of Ribs

Two types of ribs were modeled using CAD software which were then fabricated and later used for experimentation purposes.

1. Square Ribs
2. Semi-circular Ribs

These rib shapes were installed inside cylinders at equal distances.

3.1.3 Square Ribs

Square ribs were modeled using software and fabricated for the experiment. Four square ribs were installed inside the cylinder at equal distances. The dimensions of square ribs were; length: 135mm and width: 4mm.

A single square rib with dimensions is shown in Figure 3.2.

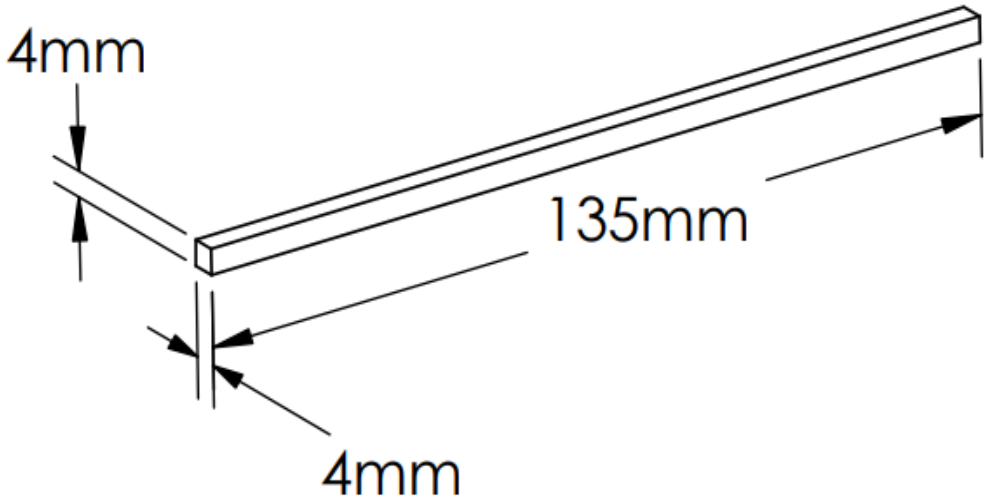

Figure 3.2: Dimensions of square rib

The dimension of the glass cylinder with semi-circular ribs installed is shown in Figure 3.3.

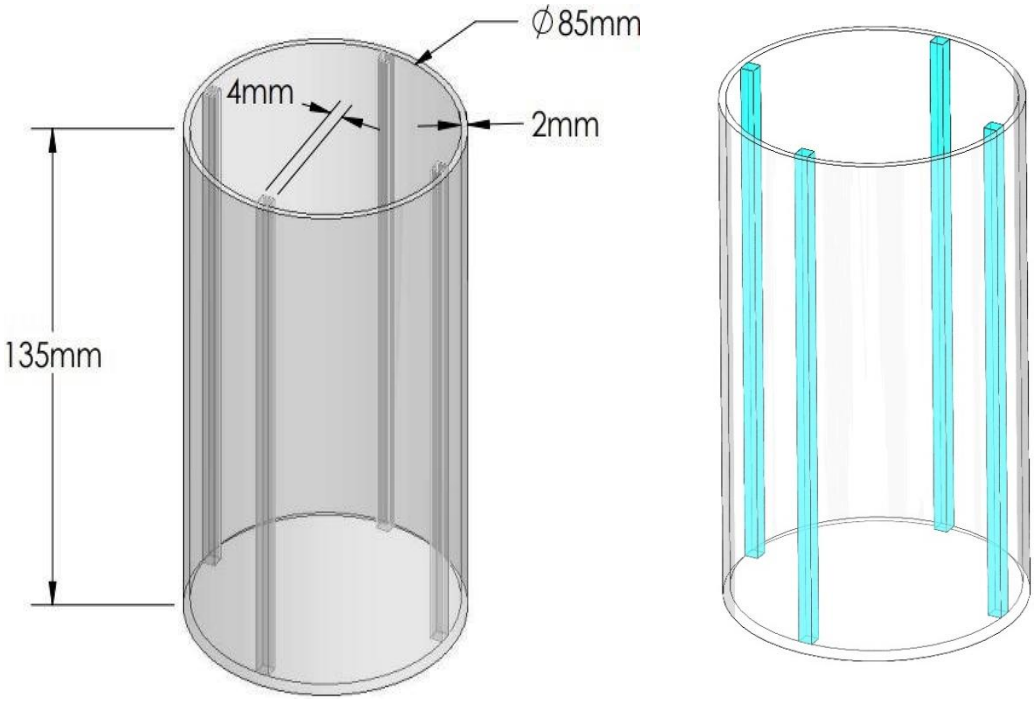

Figure 3.3: Glass cylinder with square ribs installed

3.1.4 Semi-circular Ribs

Semi-circular ribs were also modeled and fabricated for the experiment. Similar to the square ribs case, four semi-circular ribs were installed inside the cylinder at equal distances. The dimensions of a semi-circular rib were; Length: 135mm, and a radius: of 4mm.

A single semi-circular rib with the dimensions is shown in Figure 3.4.

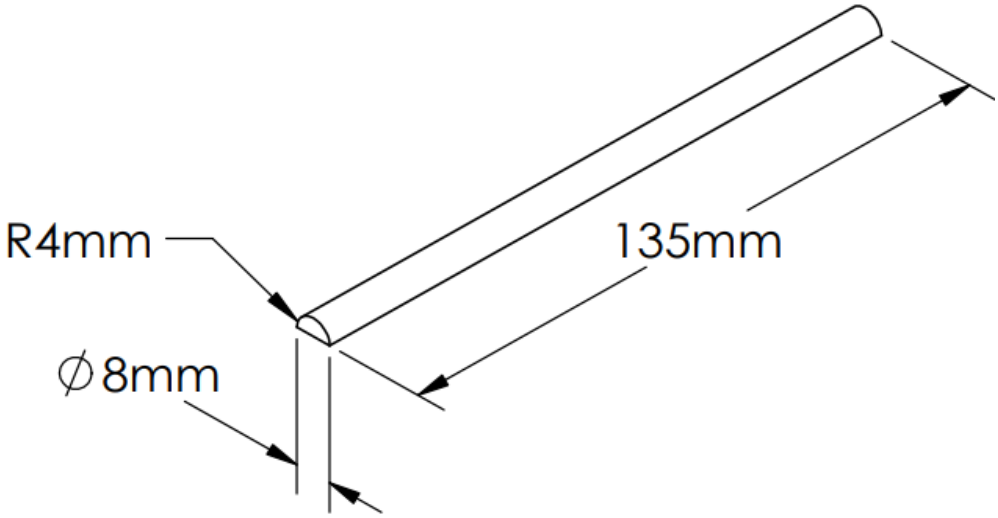

Figure 3.4: Dimensions of semi-circular rib

The dimension of the cylinder with semi-circular ribs installed is shown in Figure 3.5.

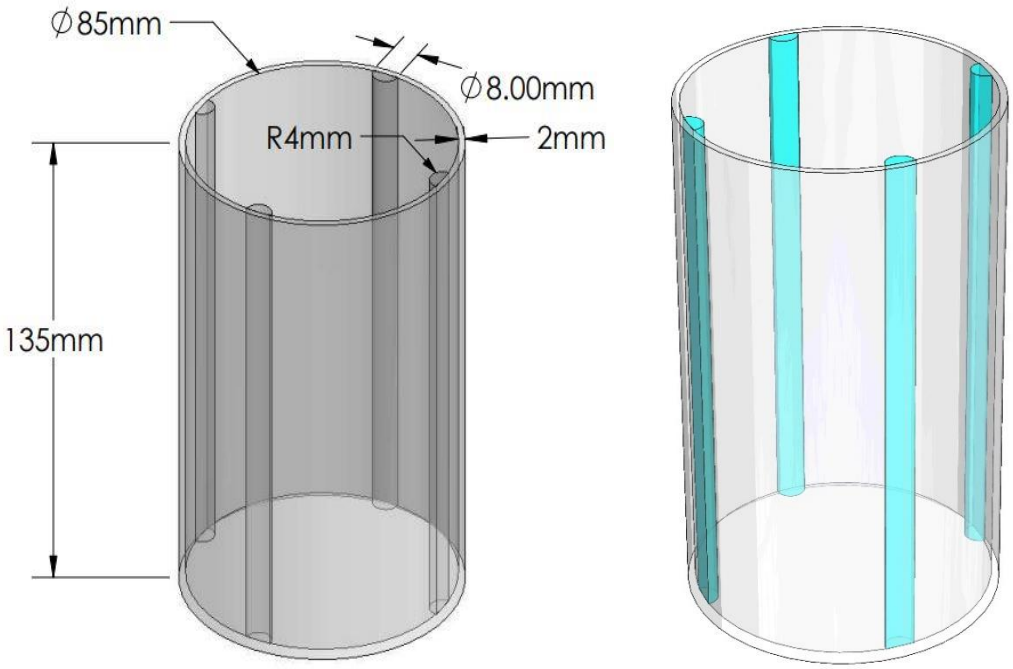

Figure 3.5: Glass cylinder with semi-circular ribs installed

3.2 Test Section Fabrication

After the design and modeling of the cylinders and ribs, the next step is the fabrication of the system. Fabrication includes various steps like cutting according to the drawing, machining, and assembling. Specially designed glass cylinders were manufactured according to the specific dimensions. The square and semi-circular ribs were

manufactured by laser cutting and lathe machines. The material used for the ribs was acrylic. Table 3.1 gives the physical specifications of the test section.

Table 3.1: Physical Specifications of Test Section

Specifications	Dimensions
Test section height (mm)	457.2
Test section width (mm)	304.8
Cylinder height (mm)	135
Cylinder inner diameter (mm)	85
Cylinder thickness (mm)	2
Square rib width (mm)	4
Square rib length (mm)	135
Semi-circular rib radius (mm)	4
Semi-circular rib length (mm)	135

After the ribs were manufactured by laser cutting and lathe machine, the next step was fixing the ribs inside the cylinders. Four square ribs were installed in evenly distributed space inside the cylinder. In the same way, four semi-circular ribs were installed inside the cylinder at an equal distance. RTV General Silicone Sealant was used to install ribs inside the cylinder, as it is a clear and transparent adhesive. The material description of the test section is given in Table 3.2.

Table 3.2: Material Description of Test Section

Parameter	Material
Test Section	Glass
Cylinder	Glass
Square Rib	Acrylic
Semi-circular Rib	Acrylic

3.3 Components of PIV

The PIV system can be divided into four main components: an injection system for tracer particles, a laser setup, an imaging setup, and a processing unit (computer). The detail about the components of the PIV system is given in the following sections.

Figure 3.6 depicts the experimental configuration for Particle Image Velocimetry measurement.

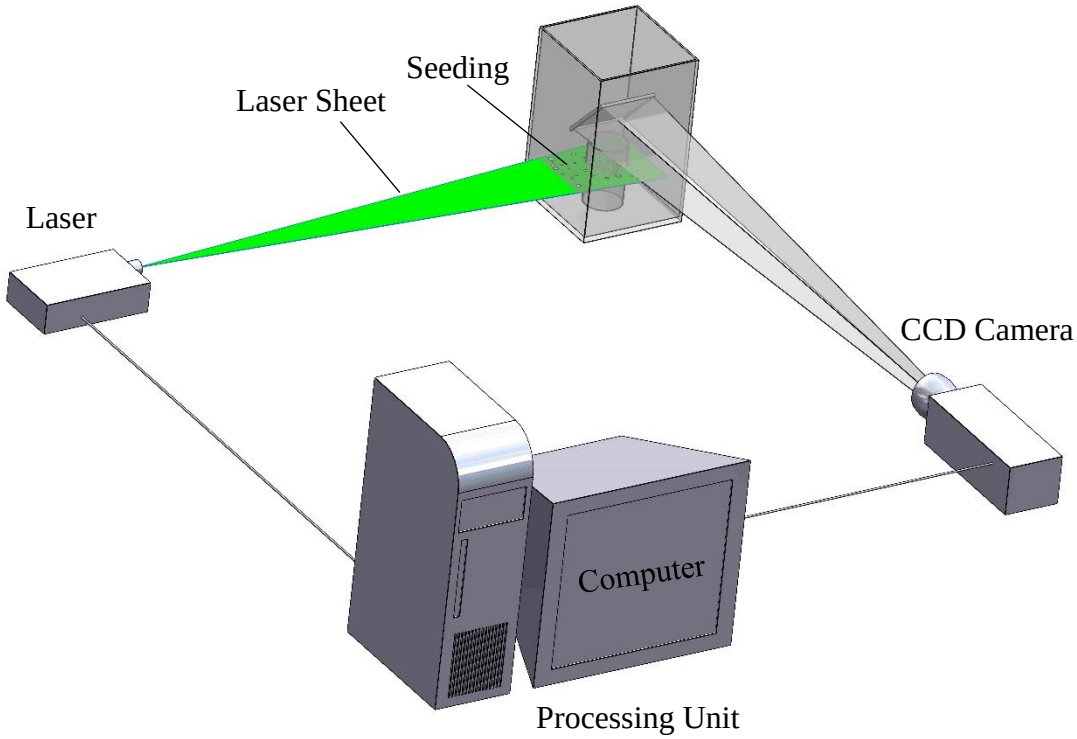

Figure 3.6: PIV experimental setup

3.3.1 Seeding the Flow with Tracer Particles

The primary and most important stage in the PIV operation is to seed the flow with tracer particles (Figure 3.7). Since PIV does not provide the velocity field of the fluid, but rather the velocity field of the tracer particles, it has a direct impact on the right approach for the PIV working. Therefore, the tracer particles must follow the flow exactly. In the present study, Hollow Glass Spheres (HGS) was used as the seeding particles. The seeding particles (HGS) have a mean diameter of 10 μm.

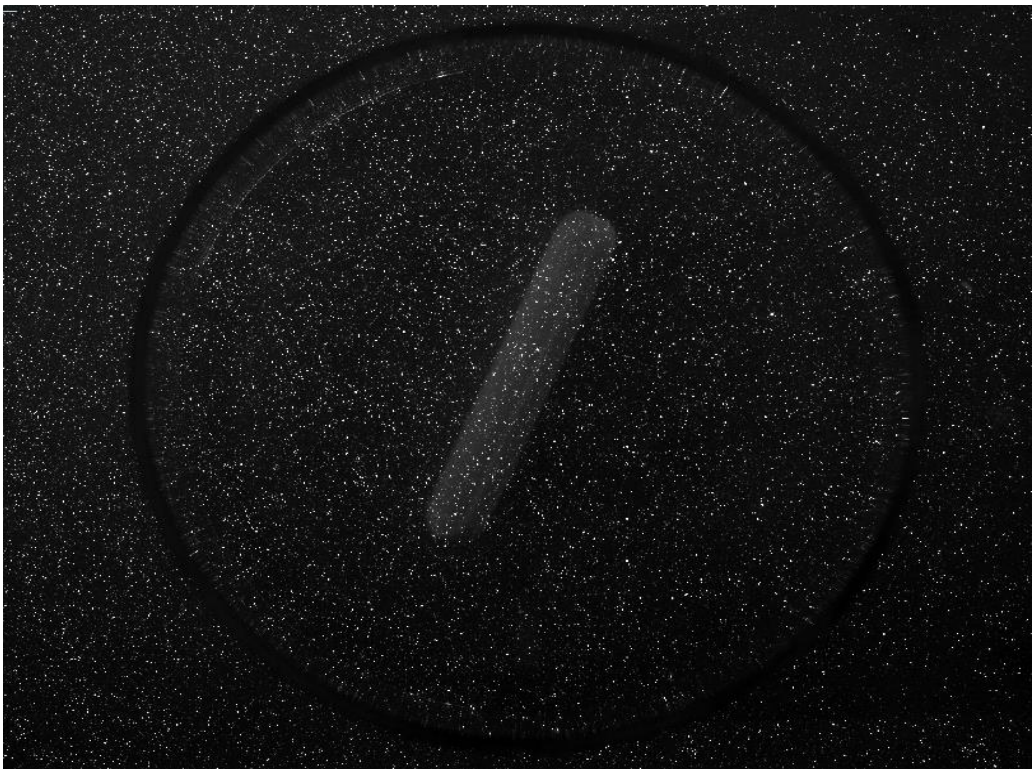

Figure 3.7: Seeding the flow with tracer particles

The following characteristics must be considered while choosing the tracer particles:

a. The buoyancy of particles should be neutral [1].
b. Particles with a higher refractive index are preferable because they disperse more light at lower intensities of light [1].
c. For obtaining better results, the size of the particles should be suitable. Neither too small that the camera cannot detect them nor too big that they change the properties of the fluid. A higher velocity lag may also be seen in the bigger size particles [2].
d. Mie scattering is greater for spherical particles than for irregular-shaped ones.
e. Not all materials are suitable for seeding particles.

To achieve the best outcomes, uniform seeding is very important. Without tracer particles, velocity cannot be determined. The inadequate seeding will cause the information to be lost and the overly seeded flow will cause speckle scattering, which will produce false findings. The characteristics of seeding particles are given in Table 3.3.

Table 3.3: Properties of Seeding Material used for Turbulent Swirl Flow [3]

Characteristics	**Specification**
	Hollow Glass Spheres
Mean particle size (µm)	10
Size distribution (µm)	2 – 20
Particle shape	Spherical
Density (g/cm^3)	1.1
Refractive index	1.52
Material	Borosilicate Glass

3.3.2 Laser Setup

The typical light source for PIV measurements is a powerful pulsed laser. Because the seeding particles are so minute, laser light is used to illuminate them to observe and find their position. To obtain images of slightly moving particles in a short time, the flow field of concern is illuminated twice at a given time interval. A double-pulsed Nd: YAG 200 class 4 laser was used for the PIV studies in this work. It was composed of two laser heads that generated laser beams in the form of a sheet with a thickness of around 2 mm. The symmetry plane of the test section is illuminated by the laser sheet, in which the CCD camera records instantaneous images. The laser generator could only operate at a maximum frequency of 15 Hz. It is the acquisition frequency and its maximum value is fixed at 15 Hz [4]. The laser that was eventually released had a wavelength of 532 nanometers, which is more receptive to cameras[5]. Table 3.4 provides the specifications of the Nd: YAG laser.

Table 3.4: Technical Specifications of Nd: YAG Laser

Parameter	Specification
Frequency(Hz)	15
Laser sheet thickness (mm)	2
Pulse width (nm)	3 - 5
Pulse duration (ns)	4
Wavelength (nm)	532
Maximum output (mJ)	1200
Beam diameter (mm)	5.5
Laser medium	Nd: YAG

3.3.3 Imaging System

When laser flashes on tracer particles, the light is scattered. The light scattering particles were captured using a 30 fps Charged Couple Device (CCD) camera, which had its optical axis perpendicular to the plane of the laser sheet. A laser sheet illuminates the flow in the target area. A high-resolution camera was used to view the detail of the area under consideration. The camera lens projects the targeted region onto the sensor array of a digital camera. Each light pulse can be captured in its image frame by the camera. Two consecutive image frames were captured with a short time interval between them to measure the displacement of particles [6]. These image frames were captured in real-time and saved instantly in the memory of the computer. A 50 mm Nikon lens was attached to a HiSense 610 PIV camera for imaging purposes in the current study. The specifications of the CCD camera are given in Table 3.5.

Table 3.5: Specifications of CCD Camera

Parameter	Specification
Camera Model	HiSense 610
Pixels (W x H)	1600 x 1200
Number of frames recorded per second (fps)	30
Lens	Nikon Zeiss 50mm
Aperture range	f/1.4
Maximum frequency	15 Hz

3.3.4 Processing Unit

A processing device that featured an Intel(R) processor and a powerful computer was used to analyze the images. The synchronization unit, the correlator unit, and the input buffer were the three basic components of this processor. Physical connectivity between the processor and other PIV instruments was made possible by the synchronization unit (laser, camera, PC). A synchronizer ensures that both the laser light pulses and the camera are in synchronization. The vector field and input buffer readings, as well as the storage of the images in the memory, was produced by the correlator unit. Commercial software DynamicStudio 5.1 (Dantec Dynamics) was used to process and analyze the obtained images.

3.4 Experimental Setup and Processing

With the completion of fabrication and assembly of the test section, it was time to arrange all components in a certain way so that they can perform their operation and tasks smoothly. A test section filled with water having seeding particles was set in front of the camera and the laser was arranged perpendicular to the camera. This proper arrangement was a part of the procedure as it could affect the accuracy of the whole setup. The experimental setup consists of a test section, a tracer particle injection system, a laser configuration, an imaging setup, and a processing unit (computer) for obtaining results.

A test section having specific dimensions was filled with water and seeding particles were uniformly mixed with water. Cylinders were placed at the base of the test section. The main reasons for using a water-filled test section were:

1. Refractive index matching
2. The camera position is from the top, so to avoid refraction caused due to non-uniform free surface.

After placing all the components in their required place, the next step was experimentation. A magnetic stirrer was used to give constant RPMs to fluid and create swirls in a way that all images could be captured flawlessly. Different RPMs like 300, 400, and 500 were given to the fluid and the laser height variations of 36mm, 66mm, and 96mm were selected. Nanoparticles, Hollow Glass Spheres (HGS) were used as seeding particles to signify the displacement of particles in the fluid to later capture it with the camera. The experimental setup for this work is shown in Figure 3.8.

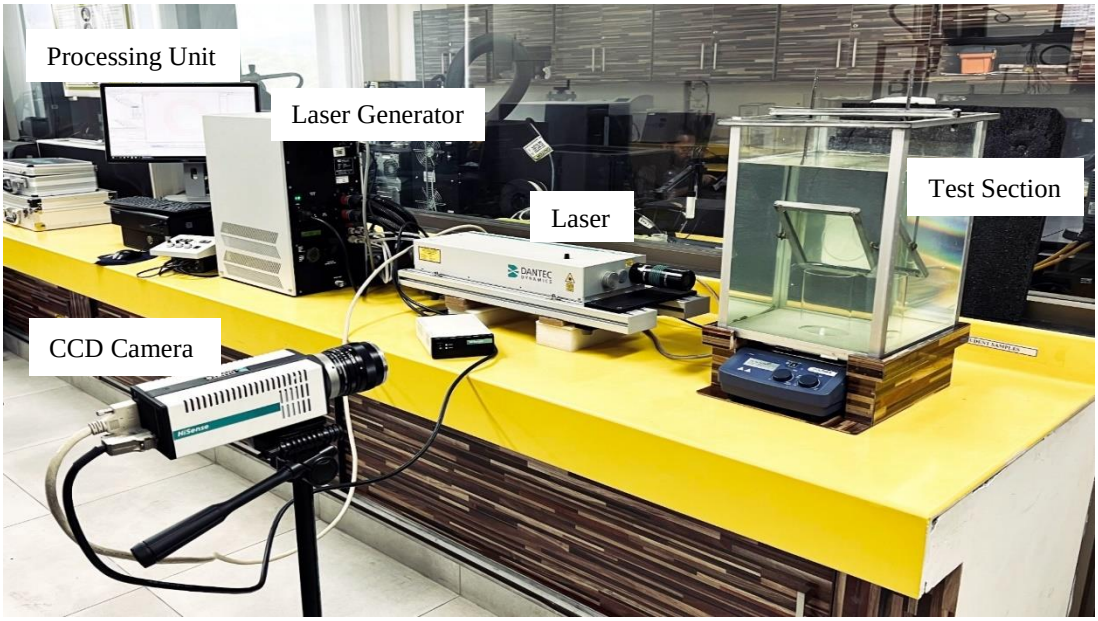

Figure 3.8: Experimental setup for Particle Image Velocimetry measurement

The Reynolds number was calculated by the formula given below (equation 3.1):

$$Re = \frac{\rho v_{avg} D_{in}}{\mu} \quad \text{…….} (3.1)$$

where,

ρ is the density of the fluid at 20°C,

v_{avg} is the average velocity of the fluid,

D_{in} is the inner diameter of the cylinder,

μ is the dynamic viscosity of the fluid at 20°C.

The Reynolds number calculations showed the highly turbulent swirl flow in this study.

Cylindrical containers were varied from plain to ribbed and tested one by one. First, the container without ribs was tested and then the square container was tested. After that, experiments in the container with semi-circular ribs were performed. Then the test section was illuminated by a laser and the movement of seeding particles was recorded by the CCD camera. A computer was used to calculate the velocity fields by determining the displacement of tracer particles in two consecutive image frames during a short interval of time.

Several experiments were conducted at various laser beam heights, initially without rib configuration and subsequently with square rib and semi-circular rib configurations. Experiments were conducted in cylinders at various water RPMs such as 300, 400, and 500. The water in the cylinder was stirred at constant RPM by a magnetic stirrer.

During experimentation, data was collected in the form of images with help of a camera and stored in the storage memory. The camera was connected to a processing unit. The raw images obtained for each swirl flow case were processed and various filters were applied to get a final vector. This was done by the DynamicStudio 5.1 software. After pre-processing and post-processing, the required data was extracted which will be explained in Chapter 5.

In this study, 100 image pairs are analyzed in each case to obtain statistical data. The PIV images were captured, processed, analyzed, and displayed on a dual processor workstation with commercial software (DynamicStudio 5.1, Dantec Dynamics).

Summary

In this chapter, the detail of the experimental setup has been discussed. The design and modeling of the test section in CAD software are given at the start of the chapter. The fabrication process is described in detail. In the next section, the assembling of manufactured cylinders and ribs has been explained. The experimental setup of PIV has also been discussed. The experiments were run by variation in the RPM and using plain and ribbed cylinders. Data was obtained which was later processed to understand the flow behavior inside the cylinders.

References

[1] R. G. T. Hadad, “Effects of particle size, concentration and surface coating on turbulent flow properties obtained using PIV/PTV,” Exp. Therm. Fluid Sci. 45 203–212, pp. 203–213, 2013.

[2] A. Melling, “Tracer particles and seeding for particle image velocimetry,” Meas. Sci. Technol., vol. 8, no. 12, pp. 1406–1416, 1997.

[3] “Seeding Materials - Dantec Dynamics | Precision Measurement Systems & Sensors.” https://www.dantecdynamics.com/components/seeding-materials/ (accessed Dec. 17, 2021).

[4] A. Caldeira-pires and R. Q. Neiva, “Swirling Flow Analysis using PIV,” Procedings COBEM 2007, p. 7, 2007.

[5] C. Brossard et al., “Principles and Applications of Particle Image Velocimetry,” Onera AerospaceLab J., vol. AL01-03, no. 1, pp. 1–11, 2009.

[6] K. Suga, S. Tominaga, M. Mori, and M. Kaneda, “Turbulence Characteristics in Flows Over Solid and Porous Square Ribs Mounted on Porous Walls,” Flow, Turbul. Combust., vol. 91, no. 1, pp. 19–40, 2013.

Chapter 4 : Particle Image Velocimetry

Particle Image Velocimetry, a non-intrusive experimental approach, is described in this chapter along with its working. The experimental configuration includes a tracer seeding system, PIV laser setup, imaging arrangement, and a computer for obtaining results. In accordance, a thorough discussion of the selection and implementation of the above-mentioned system is presented. The chapter describes in detail the basic concept of the PIV technique as well as clear and concise theory. Pre-processing, velocity vector calculation and post-processing are the three subsections that define and describe PIV processing, which is the method to construct velocity fields.

4.1 Working of Particle Image Velocimetry

In this work, the capabilities of a modern non-intrusive optical technology, particle image velocimetry (PIV), are used to acquire instantaneous flow field data from the domain of interest. PIV, which is based on the well-known relationship speed is equal to the distance over time, can provide velocity data across an entire field. In PIV, tracer particles are seeded into the flow to determine the velocity of tracers by measuring the distance traveled by particles in the flow during a given time interval [1], [2].

The tracer particles are illuminated by a laser. To precisely follow the flow, the particles should be the proper size. The tracer particles are illuminated twice with a laser light sheet to determine the displacement of particles. The illuminated tracer particles are captured by a digital camera. The measurement of particle displacement requires the capturing of two consecutive image frames. The velocity can be calculated from the displacement of the tracer particles in the second image (t_2) relative to their location in the first image (t_1) (equation 4.1) [3]–[5].

$$v = \frac{\Delta s}{t_2 - t_1} \quad \text{.....} \quad (4.1)$$

The measurement principle of PIV is shown in Figure 4.1.

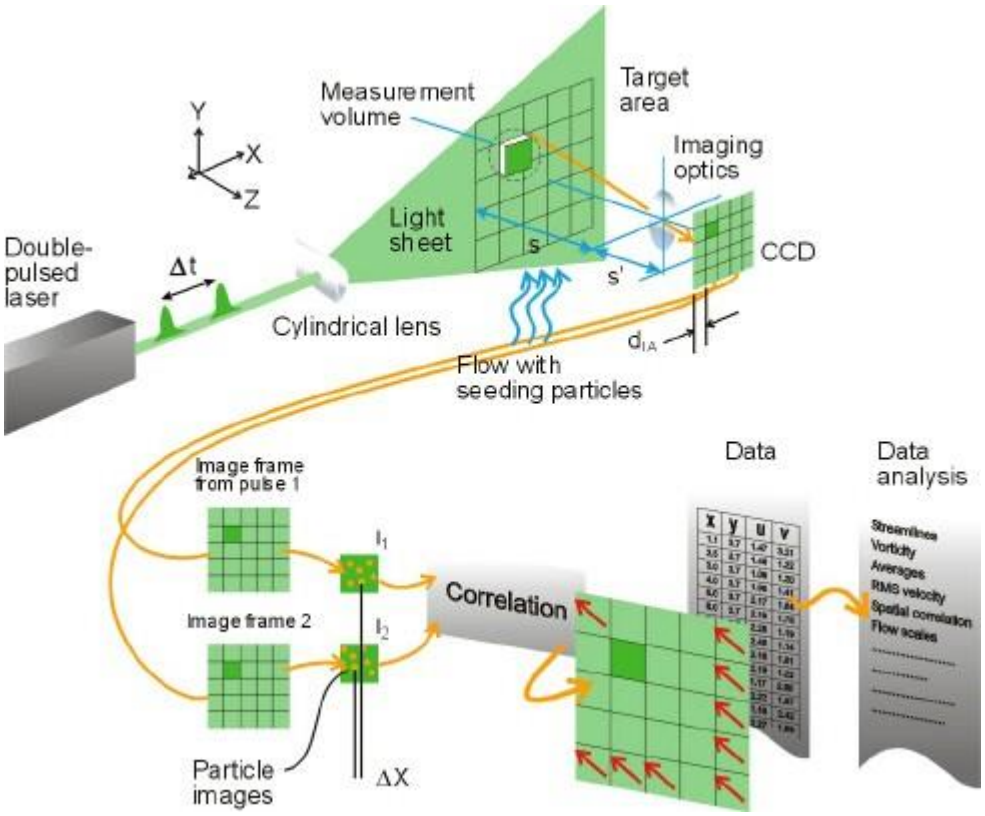

Figure 4.1: Measurement principle of PIV [6]

4.2 Processing and Application of PIV in a Cylinder

The PIV system is explained in detail in this section, along with the steps involved in creating the instantaneous entire velocity field from the raw images obtained by the CCD camera. When using the PIV setup, a highly turbulent swirl flow was taken into consideration. The seeding particles Hollow Glass Spheres (HGS) were mixed with water, which was used as the working fluid. Given that HGS has a refractive index close to that of water and a density that is almost identical to water, these particles were found appropriate for these PIV studies. The images of the light scattering tracers were taken with a double-frame CCD camera and just one camera was used for the imaging purpose. 100 double-frame images were captured and saved into the memory of a computer for PIV computation. Pre-processing, vector calculation, and post-processing are the three key phases of PIV processing. Table 4.1 gives the detail of the experimental runs used in this study.

Table 4.1: Detail of Experimental Runs

Types of Rib	Height of Laser (mm)	RPM	MSF (Absolute Distance) (mm)	Scale Factor	Time between pulses (μs)	Image pixels	Grid Step Size in Adaptive PIV
Plain case	36	300	85	12.01	1800	1600x1200	32x32
Plain case	36	400	85	12.01	1500	1600x1200	32x32
Plain case	36	500	85	12.01	1500	1600x1200	32x32
Plain case	66	300	85	11.56	1500	1600x1200	32x32
Plain case	66	400	85	11.56	1800	1600x1200	32x32
Plain case	66	500	85	11.56	2000	1600x1200	32x32
Plain case	96	300	85	11.87	1800	1600x1200	32x32
Plain case	96	400	85	11.87	2000	1600x1200	32x32
Plain case	96	500	85	11.87	1800	1600x1200	32x32
Square	36	300	85	11.32	2200	1600x1200	25x25
Square	36	400	85	11.32	2100	1600x1200	25x25
Square	36	500	85	11.32	2000	1600x1200	25x25
Square	66	300	85	11.43	2200	1600x1200	25x25
Square	66	400	85	11.43	2100	1600x1200	25x25
Square	66	500	85	11.43	2000	1600x1200	25x25
Square	96	300	85	11.57	2200	1600x1200	25x25
Square	96	400	85	11.57	2200	1600x1200	25x25
Square	96	500	85	11.57	2100	1600x1200	25x25
Semi-circular	36	300	85	12.43	2200	1600x1200	25x25
Semi-circular	36	400	85	12.43	2200	1600x1200	25x25
Semi-circular	36	500	85	12.43	2100	1600x1200	25x25
Semi-circular	66	300	85	11.9	2200	1600x1200	25x25
Semi-circular	66	400	85	11.9	2200	1600x1200	25x25
Semi-circular	66	500	85	11.9	2100	1600x1200	25x25
Semi-circular	96	300	85	11.49	2200	1600x1200	25x25
Semi-circular	96	400	85	11.49	2200	1600x1200	25x25
Semi-circular	96	500	85	11.49	2100	1600x1200	25x25

4.3 Pre-Processing

The PIV processing began with the sequence of images that were saved in real-time in the computer memory. An interrogation window is another name for an image frame. Furthermore, the interrogation window was resized into interrogation areas (IA), which are small resolution regions (Figure 4.2).

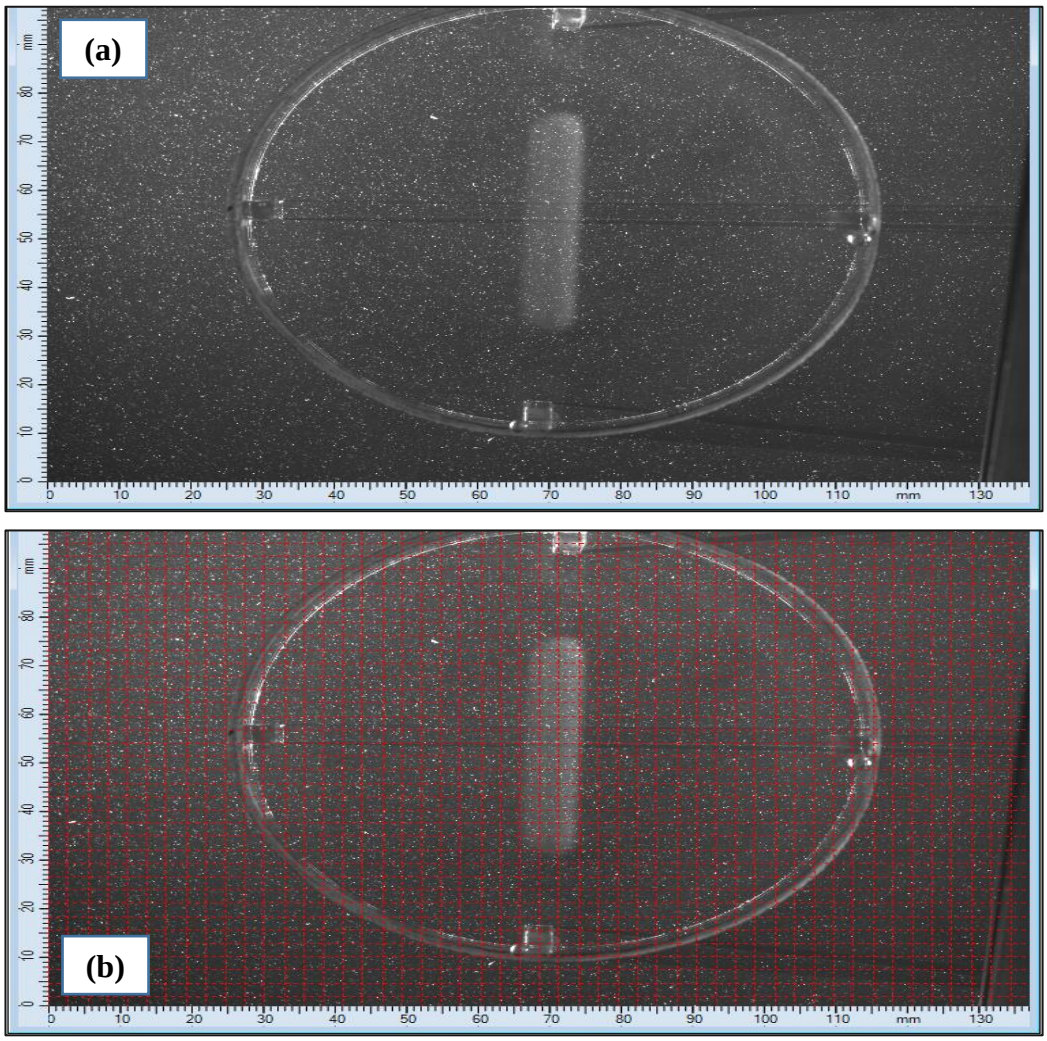

Figure 4.2: (a) Raw image (b) small interrogation areas of 32 x 32 pixels for subsampling

Pre-processing frequently assisted in enhancing image quality and increasing the signal-to-noise ratio. The causes of the background noise in the interrogation window were typically several reflections of the particles and the ambient light. This gradually decreased the signal-to-noise ratio. Therefore in this study, a pre-processing procedure that involved subtracting the background signal intensity and masking out the undesirable area was used for the raw images (Figure 4.3). The pixel intensities of the 100 images obtained were averaged to find a common image, which was then

subtracted from all of the sampled images. As a result, the signal-to-noise ratio increased after the background noise was removed. Ultimately, to prevent false findings, the undesirable areas with intense laser light were masked out (Figure 4.3).

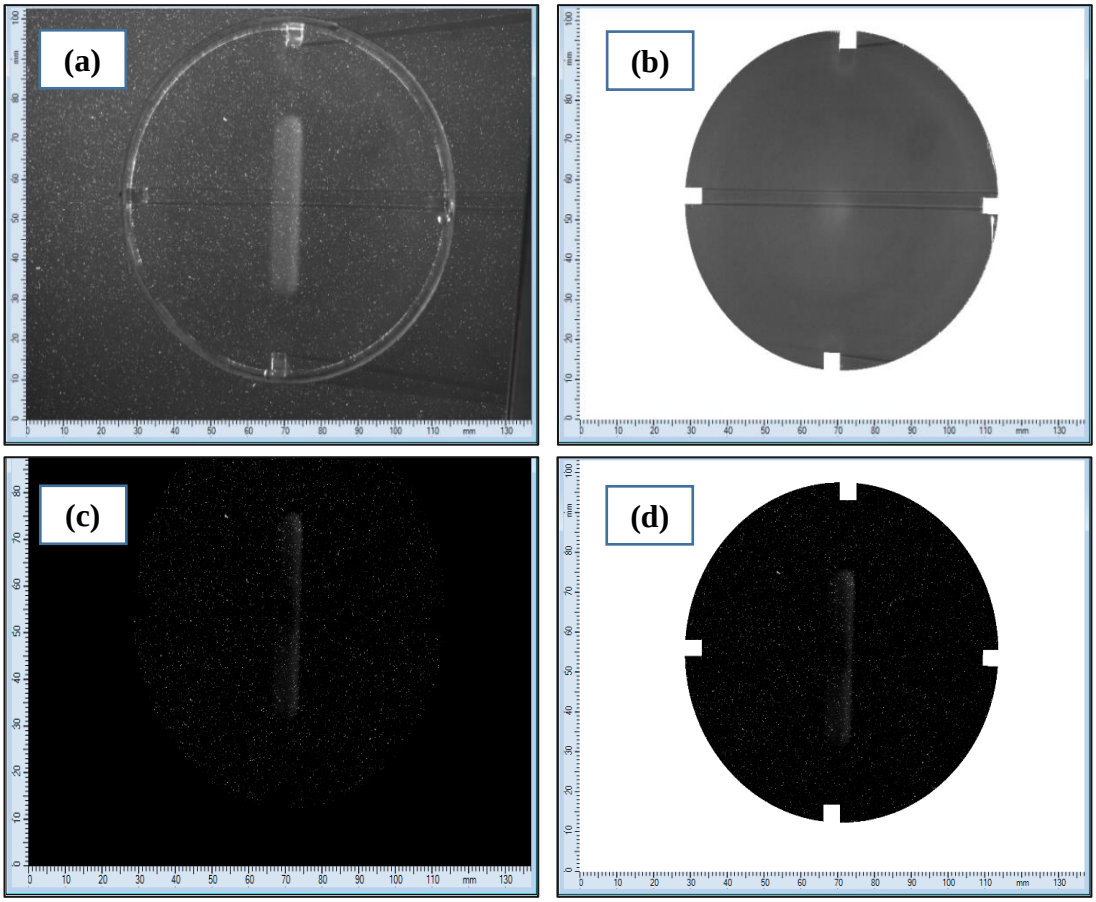

Figure 4.3: Increasing the signal-to-noise ratio through preprocessing of (a) a raw image by subtracting (b) the average image intensity (constant background noise and outliers). The undesired regions from (c) a subtracted image were then (d) masked out

4.3.1 Vector Calculation

The dimension of an IA in the object space determines how many vectors are present in an interrogation plane in PIV, which uses the cross-correlation computation method. IAs are typically available in sizes of 16 x 16, 32 x 32, 64 x 64, or 128 x 128 pixels. When choosing the size of an IA, the following factors should be taken into account.

a. In the region under consideration, a minimum of 5 seeding particles must be present to provide an optimum correlation result.
b. The distance between the particles of the subsequent images should not be more than one-fourth of the IA size to achieve good measurement precision.

c. An IA's size should be sufficient to adequately encompass the maximum dynamic range of velocity values.

32 x 32 pixels which is a good cross-correlation interrogation area size was utilized in the current work (Figure 4.2). Cross-correlation is a method for calculating the average spatial displacement of the seeding particles from one displaced image frame to its equivalent in the subsequent frame inside the IA. A basic system known as the linear digital signal processing system can be used to explain this spatial change. The function $i_1\ (m, n)$ describes the intensity of light measured at time t within the IA, while the function $i_2\ (m, n)$ describes the intensity of light measured at time $t + \Delta t$ for the second image. Where (m, n) denotes the location of a pixel within an IA and the capitalized functions are their equivalent lower-case Fourier transformations of functions, where (u, v) stands for the positional frequency field coordinates.

Using the values of $i_1\ (m, n)$ and $i_2\ (m, n)$, the primary objective of PIV is to approximate the spatial shift function $s\ (m, n)$. However, issues result due to the additive nature of the noise. A statistical method known as spatial cross-correlation calculates the spatial shift function $s\ (m, n)$. A raw vector map is produced over an entire field plane after the average spatial shift has been determined in an IA.

Cross-correlation was used to produce the raw vector maps of 100 obtained images, utilizing the Fast Fourier Transfer (FFT) algorithm-based DynamicStudio 5.1 software.

4.4 Post-Processing

Cross-correlation generates the raw velocity vector fields, which makes it simple to identify invalid vectors. These invalid vectors may differ in size or have a different direction from their surrounding area as shown in Figure 4.4 (a). Hence, a validation process should be applied to these raw vector fields to identify and substitute the outliers. The moving average validation approach and the average filtering technique were used in the current work to cope with the invalid vectors.

4.4.1 Moving Average Validation

The moving-average validation method compares the invalid vectors to their surrounding vectors to determine whether to accept or reject them. Vectors are neglected or substituted with an assumption based on the surrounding values under the premise that the behavior of the flow field is continuous. To prevent too much deviation of a vector from its nearby vectors, it is intended that the velocity field should

vary very slowly. Consequently, a relation between a vector and the vectors around it should exist. As a result, a vector must be an invalid vector if the deviation from its immediate surroundings is excessive. A rectangular neighborhood (m x n) to the vector grid is initially specified in moving-average validation. In this work, a window size of 5 x 5 vector was selected and following which each vector is correlated to the moving average of all the vectors in this neighborhood.

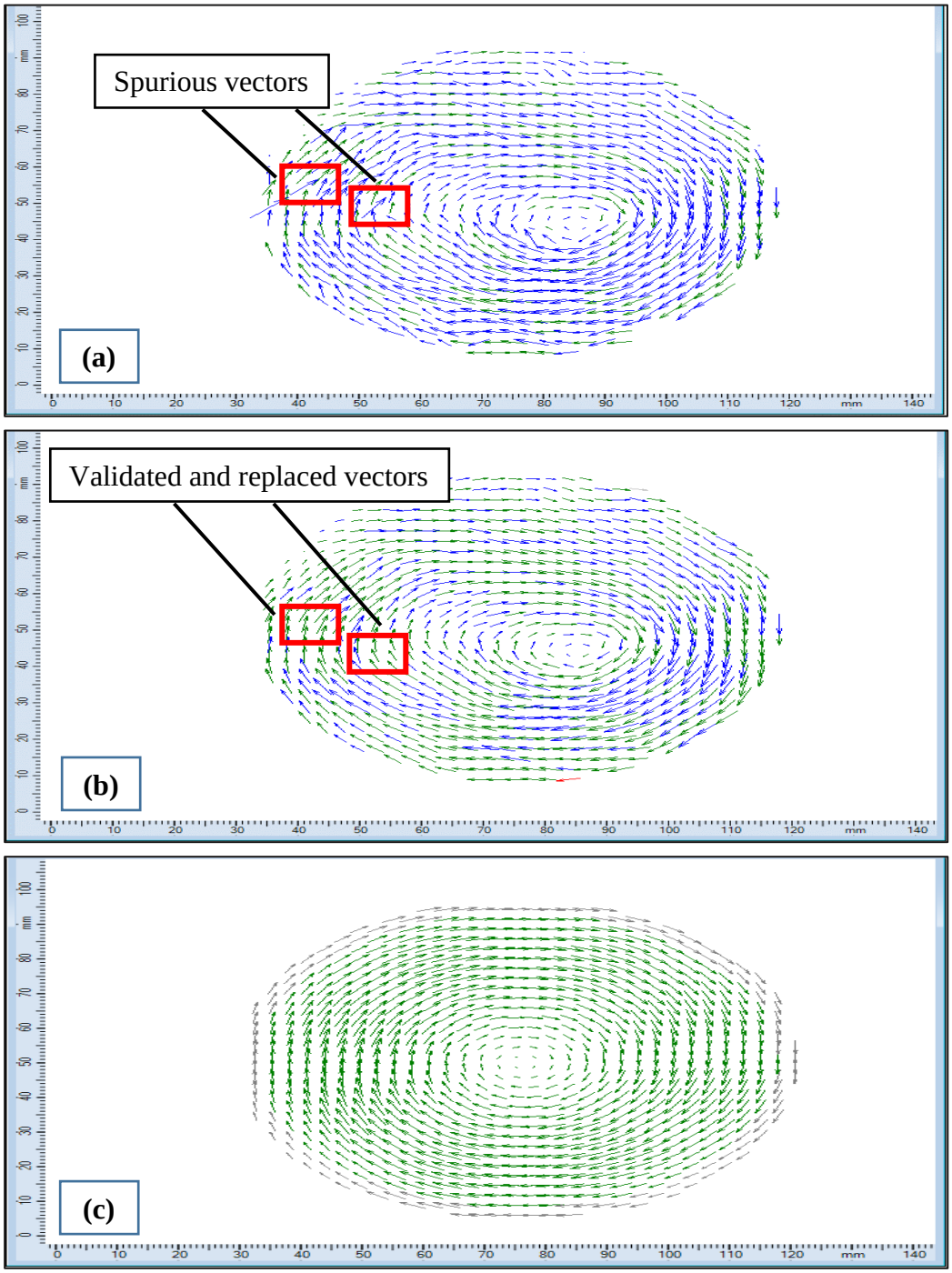

Figure 4.4: (a) Raw vector map with invalid vectors that were validated by (b) moving average validation and (c) additional moving average filter was applied to minimize noise

Overall 100 raw vector maps were subjected to a moving average validation having a rectangular grid dimension of 5 x 5 vectors, and the invalid vectors were successfully validated and substituted by applying the iterative interpolation method as shown in Figure 4.4 (b).

4.4.2 Moving Average Filter

The noise that could cause some inaccuracies in the direction and size was reduced using filter functions. Noise is considered to be any fluctuation in velocity within an interrogating area. When conducting mathematical derivations such as those involving vorticity, introducing the filter can efficiently limit the effect of noise. The verified vector field is always used to apply these filters. To reduce noise, a moving average filter was used in this work, Figure 4.4 (c).

4.5 PIV Results

The instantaneous velocity field of turbulent swirl flows in cylinders was measured using initial PIV research. 100 sets of valid vector fields were obtained by employing the validation method stated above. Figure 4.5 (a-b) shows an ensemble average vector field of 100 validated vector fields as well as the scalar total velocity field respectively.

100 images were obtained for each swirl flow case and pre-processing and post-processing techniques were applied to them. After pre-processing and post-processing of captured images, valid vector fields were obtained and further analyzed. There are various options in DynamicStudio 5.1 software to obtain various parameters like velocity, vorticity, swirl strength, turbulent intensity, etc.

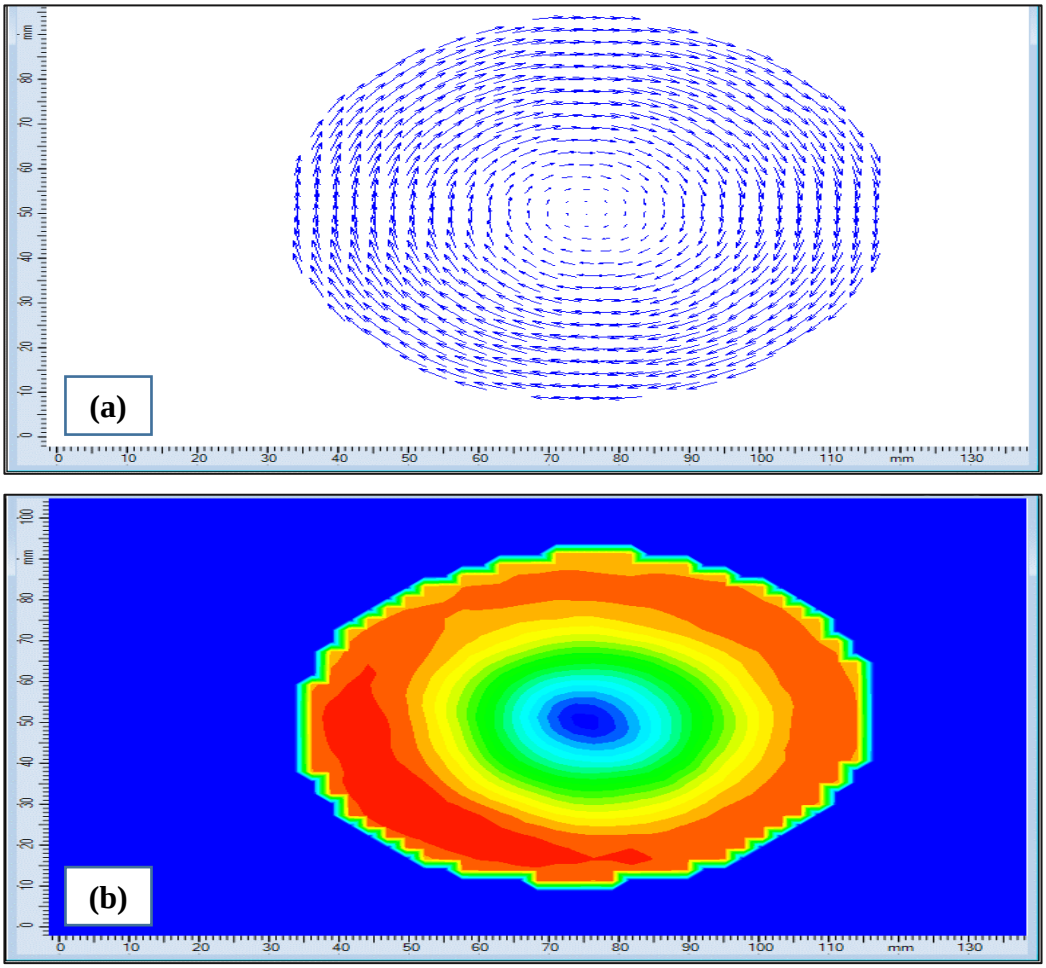

Figure 4.5: (a) Ensemble average vector field and (b) the scalar total velocity field

Summary

In this chapter, the working of an experimental technique PIV is explained in detail. This chapter also provides an initial analysis of PIV using the measurement of a turbulent flow field in cylinders. The flow is introduced with appropriate tracer particles that have the same density as that of the fluid.

A CCD camera captures images of the particles floating in the probing field after the tracer particles are illuminated by a laser sheet. The movement of the particles was determined using a statistical cross-correlation approach after the image frame was divided into discrete interrogation areas. The displacement throughout the time among the two images is all that determines the velocity for each investigating region.

The captured images were adjusted and the signal-to-noise ratio was increased by applying the pre-processing techniques. The cross-correlation method was applied to determine the average displacement of the seeding particles, and thus a raw vector map was obtained. The post-processing techniques were applied to fix the raw vector map outliers. The test section was then used to test the operation of PIV for the turbulent swirl flow.

References

[1] C. Brossard et al., “Principles and Applications of Particle Image Velocimetry,” Onera AerospaceLab J., vol. AL01-03, no. 1, pp. 1–11, 2009.

[2] H. Chen, K. Hu, P. Cui, and X. Chen, “Investigation of vertical velocity distribution in debris flows by PIV measurement,” Geomatics, Nat. Hazards Risk, vol. 8, no. 2, pp. 1631–1642, 2017.

[3] M. D. Atkins, Velocity Field Measurement Using Particle Image Velocimetry (PIV). Elsevier Inc., 2016.

[4] R. Lindken and S. Burgmann, Laser-optical methods for transport studies in low temperature fuel cells. Woodhead Publishing Limited, 2012.

[5] L. Aanen and J. Westerweel, Measurements on the mixing of a passive scalar in a turbulent pipe flow using DPIV and LIF. Woodhead Publishing Limited, 1999.

[6] “Measurement Principles of PIV - Dantec Dynamics | Precision Measurement Systems & Sensors.” https://www.dantecdynamics.com/solutions-applications/solutions/fluid-mechanics/particle-image-velocimetry-piv/measurement-principles-of-piv/ (accessed Jan. 13, 2022).

Chapter 5 : Results and Discussion

After the experimentation, the raw data were obtained and analyzed. Pre-processing and post-processing techniques were applied to obtain plots of velocity and the contours of velocity, vorticity, and swirl strength were obtained. By comparing all results, the effect of ribs on the mixing phenomenon can be determined.

5.1 Velocity Plots

The velocity versus radius plot for swirl flow plain case at height H = 96mm and 300, 400, and 500 RPMs is shown in Figure 5.1. As expected, with the increase in RPM, the velocity also increases. The velocity near the center of the cylinder is minimum and the velocity nearly approaches zero at the cylinder wall due to wall friction. Velocity for the swirl flow plain case is maximum at 500 RPM. The velocity for all three RPM cases follows the same trend.

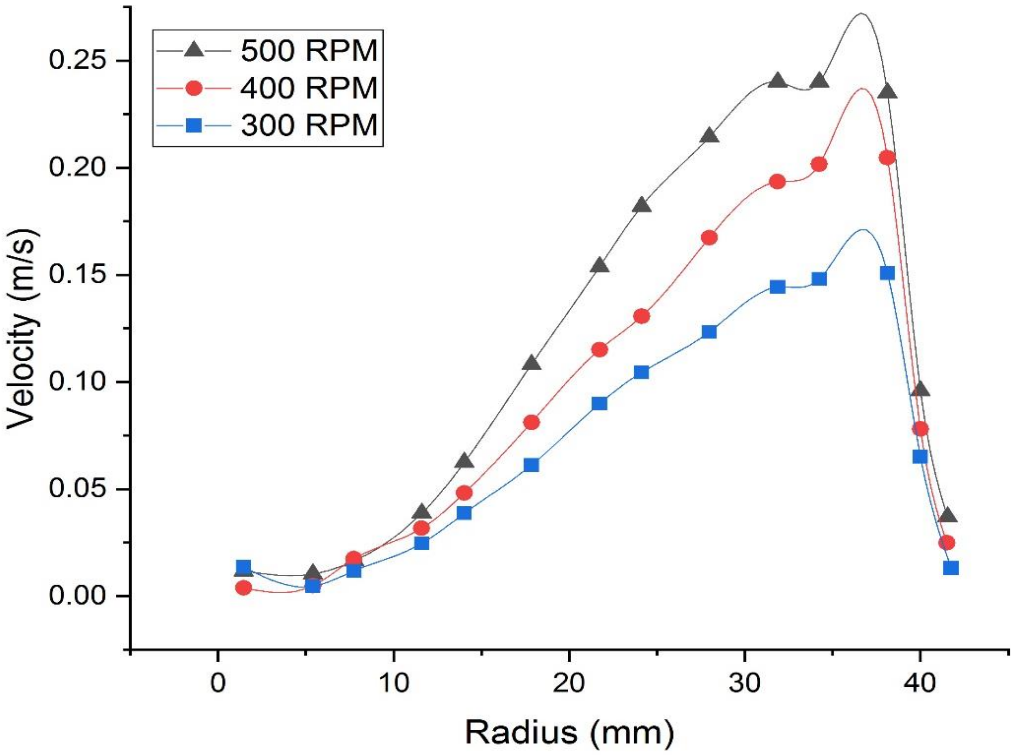

Figure 5.1: Velocity vs Radius profile plot for swirl flow plain case at H = 96mm and 300, 400, and 500 RPM

The velocity versus radius plot for swirl flow square ribs case and height H = 66mm and 300, 400, and 500 RPMs is shown in Figure 5.2. As in the swirl flow plain case, the velocity increases with the increase in RPM.

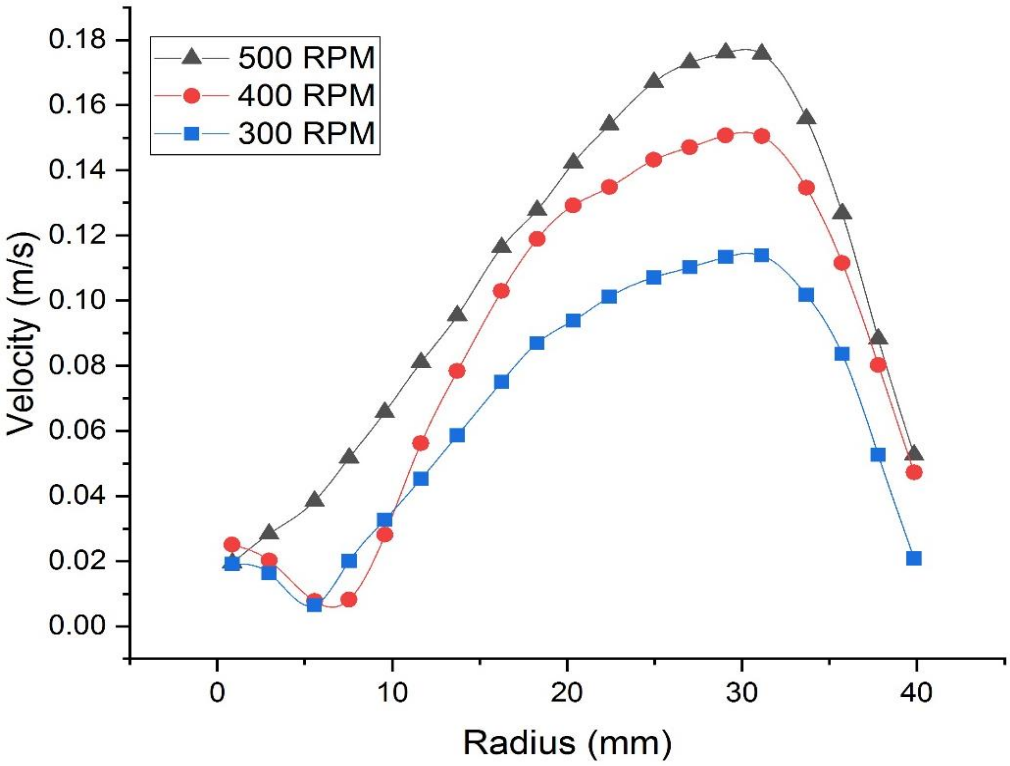

Figure 5.2: Velocity vs Radius profile plot for square ribs case at H = 66mm and 300, 400, and 500 RPM

The velocity versus radius plot for swirl flow semi-circular ribs case at height H = 66mm and 300, 400, and 500 RPMs is shown in Figure 5.3. As in the swirl flow plain case, and square ribs case the velocity increases with the increase in RPM. Furthermore, in this case, the behavior of velocity is similar to the swirl flow plain and square ribs cases.

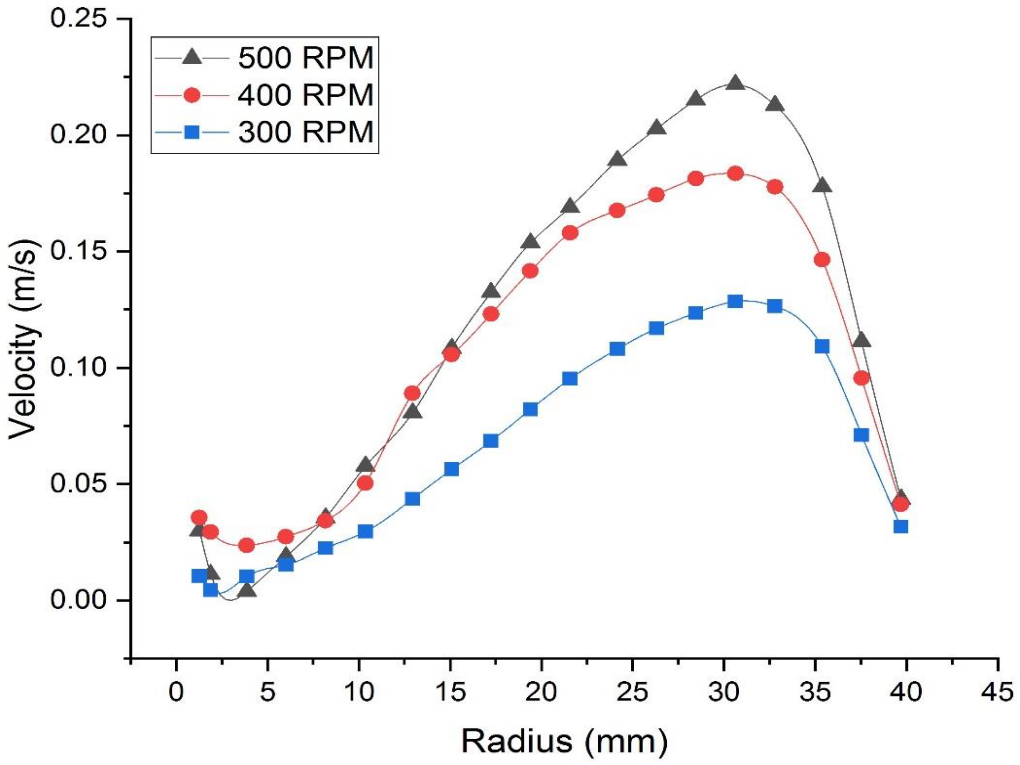

Figure 5.3: Velocity vs Radius profile plot for semi-circular ribs case at H = 66mm and 300, 400, and 500 RPM

It can be seen from the velocity plots that velocity depends on RPM and it also shows that near the center of the cylinder, the velocity nearly approaches zero due to wall friction. 500 RPM velocity plot spike shows the effect of velocity and velocity is highly dependent on revolutions per minute. However, velocity is increasing and the behavior of the plot is certain and almost similar which depicts that moving along the radial direction, all velocities follow the same trend.

The behavior of maximum velocity for swirl flow plain case is obvious. This increase in velocity is due to the reason that there is no rib inside the cylinder in the plain case. The flow does not face any obstacle and its velocity increases. But in the ribbed cases, velocity is less than that of the plain case.

5.1.1 Comparison of Velocity Plots

The comparison of velocity plots among swirl flow plain, square ribs, and semi-circular cases at different RPMs and heights of the laser beam is presented in this section.

The velocity versus radius comparison plot for swirl flow plain, square ribs, and semi-circular ribs case and height H = 36mm and 300 RPM is shown in Figure 5.4. The

velocity for the swirl flow plain case is maximum, and the velocity for the swirl flow square ribs case is minimum of all the compared cases. In plain case, the radius near the center shows up a spike in velocity. But velocity variation at the center for ribbed cases can cause more mixing than in the plain case.

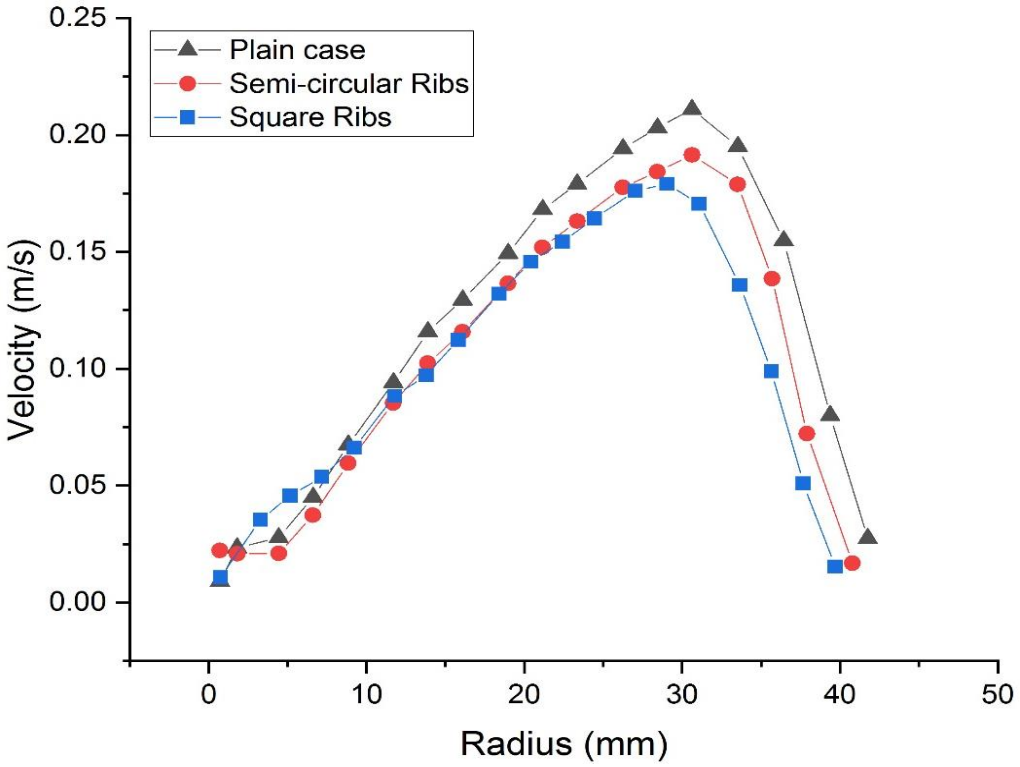

Figure 5.4: Comparison of Velocity vs Radius profile plot for swirl flow plain, square ribs, and semi-circular ribs case at H = 36mm and at 300 RPM

The velocity versus radius comparison plot for swirl flow plain, square ribs, and semi-circular ribs case and height H = 66mm and 400 RPM is shown in Figure 5.5. The velocity for the swirl flow plain case is maximum, and the velocity for the swirl flow square ribs case is minimum of all the compared cases.

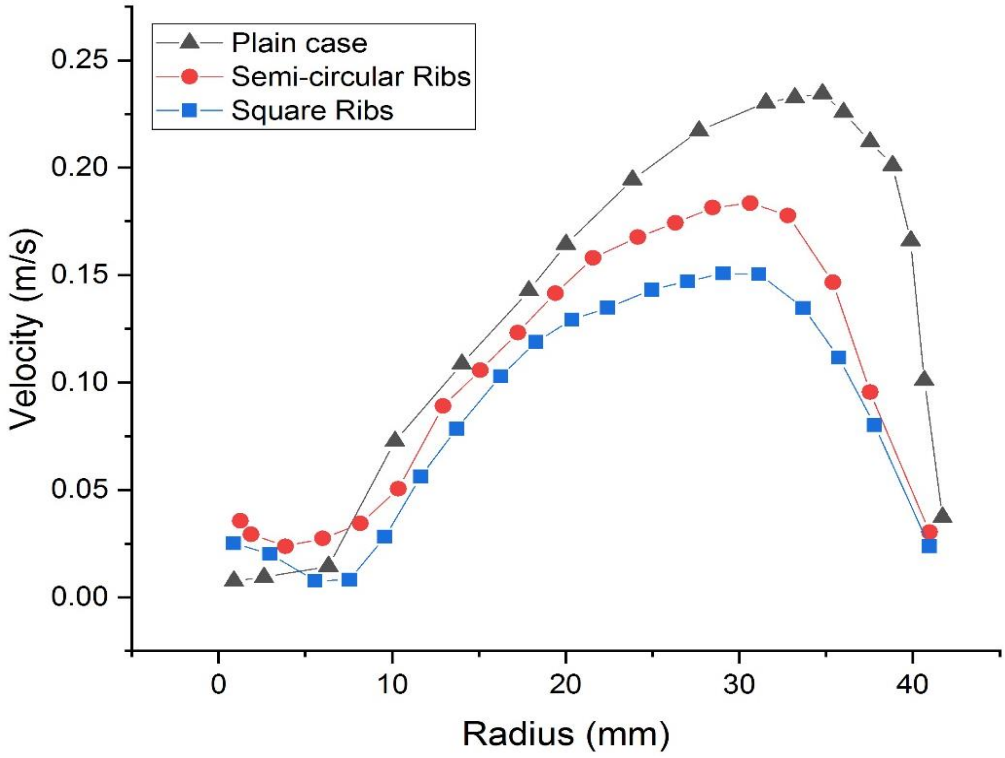

Figure 5.5: Comparison of Velocity vs Radius profile plot for swirl flow plain, square ribs, and semi-circular ribs case at H = 66mm and at 400 RPM

The velocity versus radius comparison plot for swirl flow plain, square ribs, and semi-circular ribs case and height H = 96mm and 500 RPM is shown in Figure 5.6.

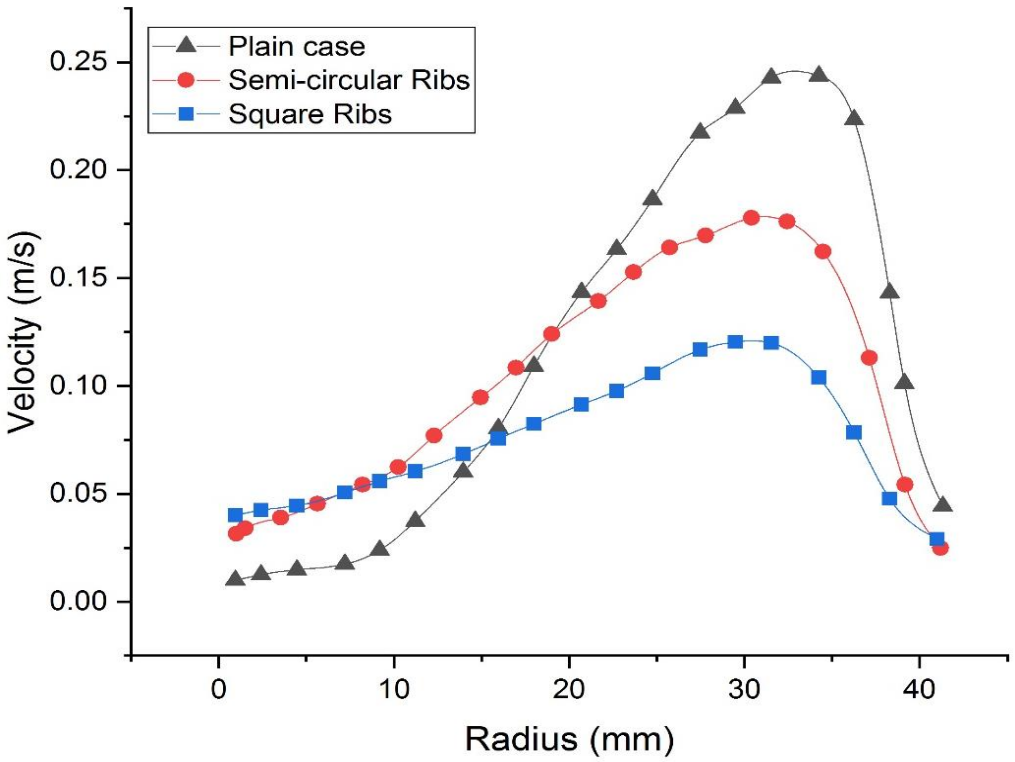

Figure 5.6: Comparison of Velocity vs Radius profile plot for swirl flow plain, square ribs, and semi-circular ribs case at H = 96mm and at 500 RPM

The velocity profile for all the compared cases is almost similar in trend, and the velocity for the swirl flow square ribs case is the minimum of all the compared cases. It can be seen from the compared profile plots that the swirl flow plain case has the maximum velocity for all the comparisons made. This is because the flow is rotated smoothly with the increase in RPM for the swirl flow plain case. While in square ribs and semi-circular ribs cases, velocity is less as compared to the plain case. The flow in the semi-circular case ribs case is somewhat smooth relative to the square ribs case. That's why its velocity is greater than the square ribs case.

5.2 Velocity Contours

In this section, the velocity contours for the swirl flow plain, square ribs, and semi-circular ribs cases at different heights of laser and 300, 400, and 500 RPMs are discussed. Furthermore, the comparison of velocity contours for all the above-mentioned cases is presented.

The contour plots of velocity for the swirl flow plain case have been shown in Figure 5.7 for 300, 400, and 500 RPMs at height H = 96mm. It can be seen that the velocity gradually increases outwards from the center of the cylinder. The velocity in the

cylinder for 300 RPM is less as compared to 400 and 500 RPM, and it increases as the RPM increases. Velocity is nearly equal to zero near the cylinder wall.

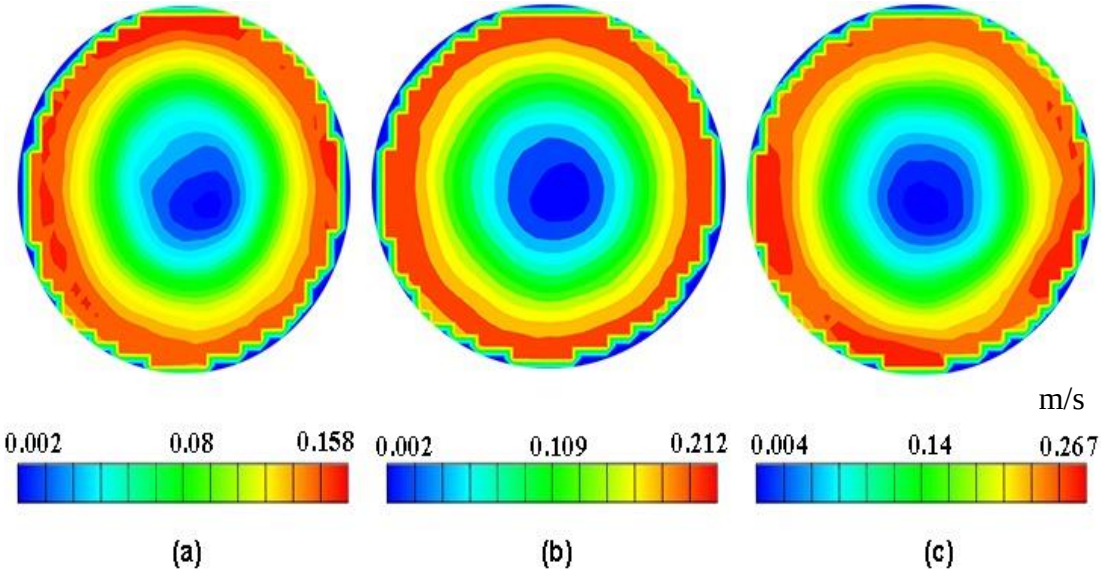

Figure 5.7: Velocity contour plots for swirl flow plain case at H = 96mm and a) 300 RPM, b) 400RPM, and c) 500 RPM

The velocity contour plots for swirl flow square ribs have been shown in Figure 5.8 for 300, 400, and 500 RPMs at height H = 66mm. Similar to the swirl flow plain case, the velocity also increases outwards from the center of the cylinder, but velocity tends to slow down just before the square ribs. Velocity increases slowly after the rib and it again decreases before the next square rib.

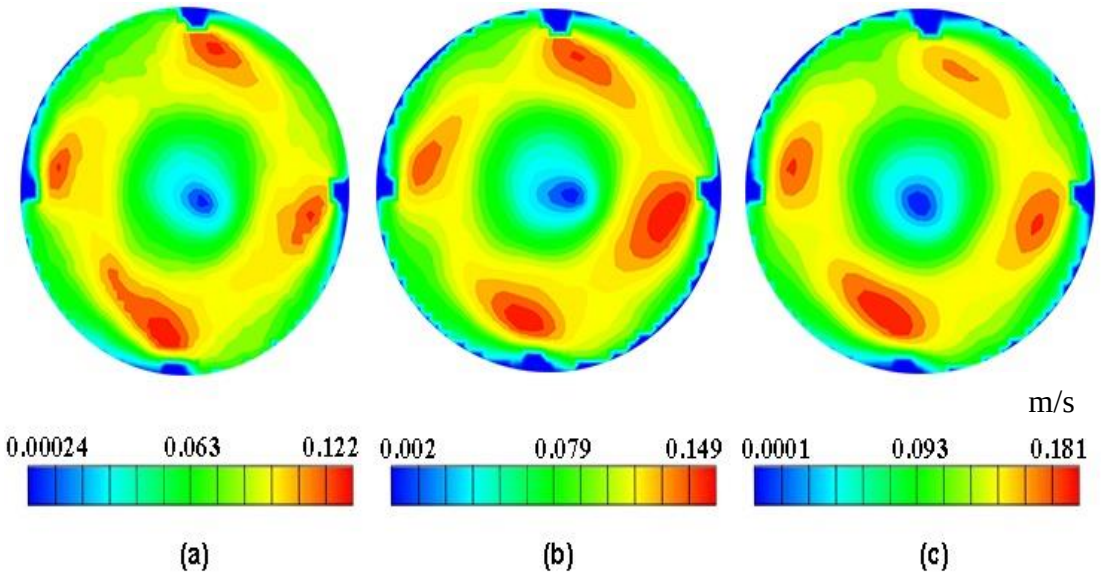

Figure 5.8: Velocity contour plots for swirl flow square ribs case at H = 66mm and a) 300 RPM, b) 400 RPM, and c) 500 RPM

The velocity contour plots for swirl flow semi-circular ribs have been shown in Figure 5.9 for 300, 400, and 500 RPMs at height H = 66mm. Velocity tends to slow down just before the semi-circular rib. Velocity increases gradually after all ribs and it again decreases before the next semi-circular rib.

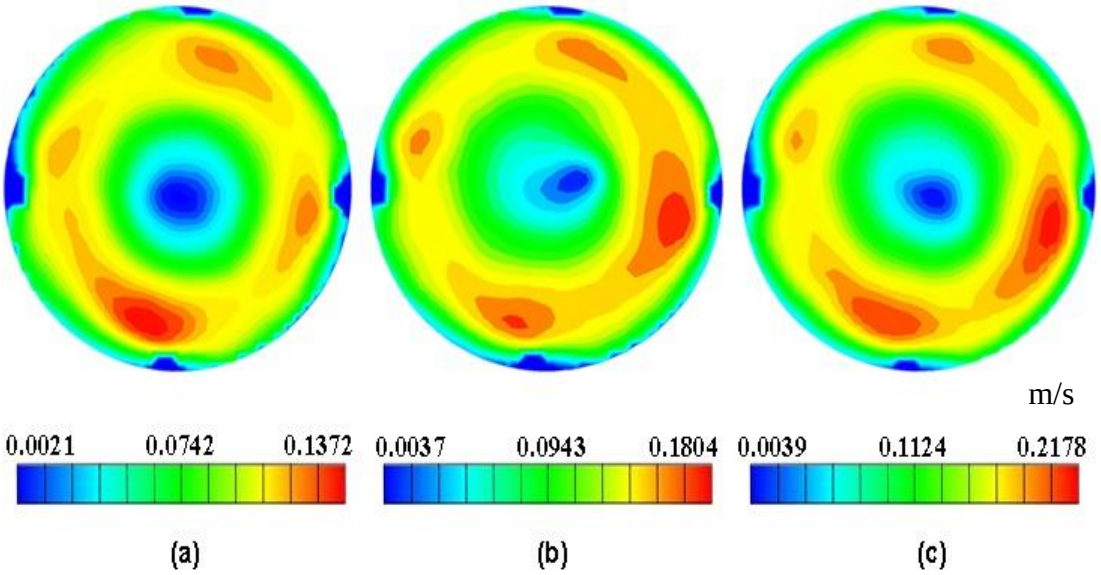

Figure 5.9: Velocity contour plots for swirl flow semi-circular ribs case at H = 66mm and a) 300 RPM, b) 400RPM, and c) 500 RPM

5.2.1 Comparison of Velocity Contours

The comparison of velocity contour plots for swirl flow plain, square rib, and semi-circular rib cases have been shown in Figure 5.10 for 300 RPM at height H = 36mm. The velocity for the swirl flow plain case is maximum. The velocity for the semi-circular ribs case is greater than the square ribs case but less than the plain case.

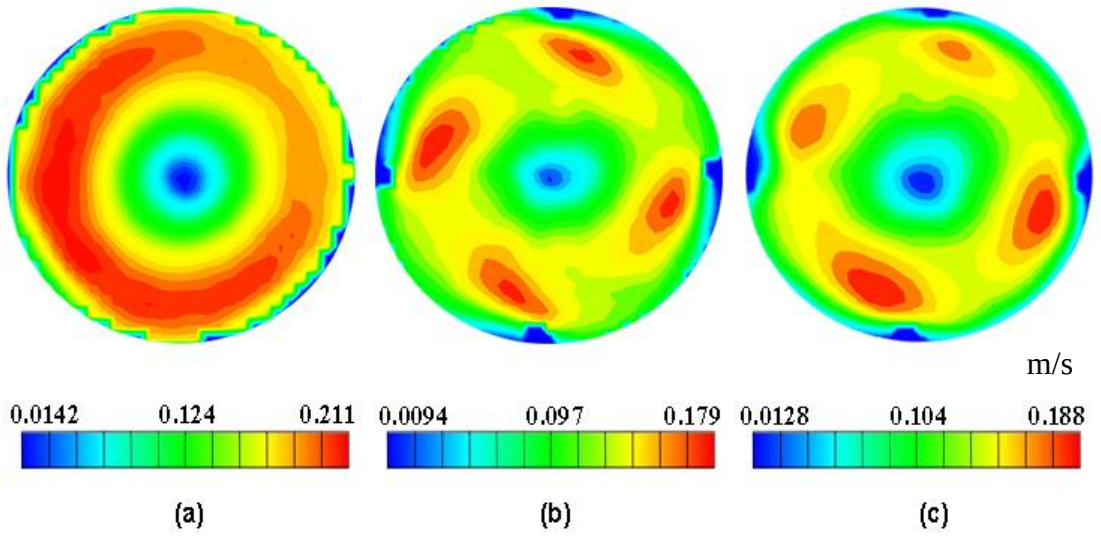

Figure 5.10: Comparison of velocity contours for a) swirl flow plain, b) square ribs, and c) semi-circular ribs case at H = 36mm and 300 RPM

The comparison of velocity contour plots for swirl flow plain, square ribs, and semi-circular ribs cases have been shown in Figure 5.11 for 400 RPM at height H = 66mm. The velocity for the swirl flow plain case is maximum. The velocity for the semi-circular ribs case is greater than the square ribs case but less than the plain case.

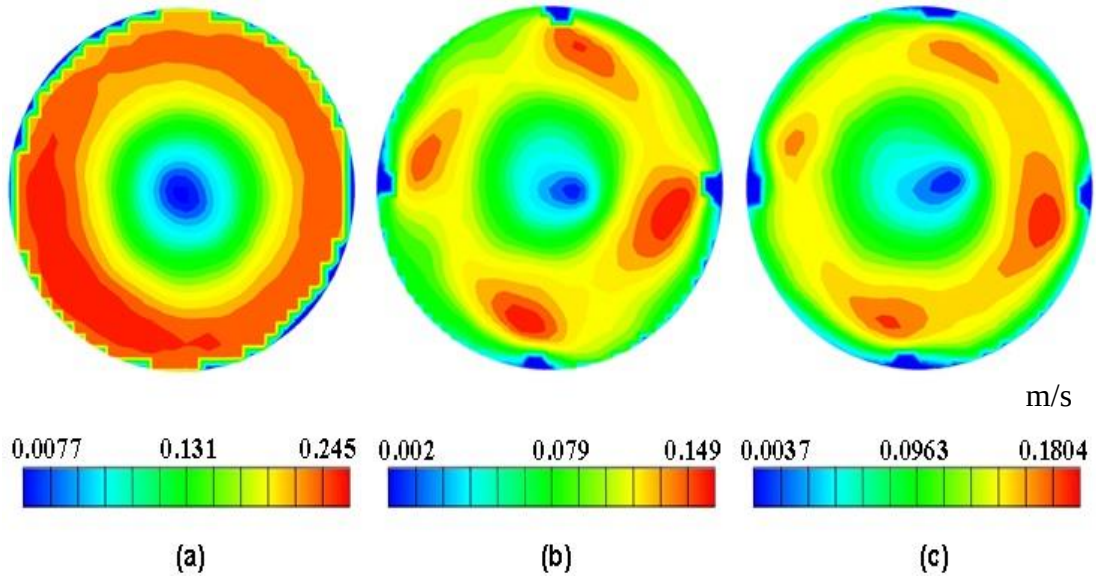

Figure 5.11: Comparison of velocity contours for a) swirl flow plain, b) square ribs, and c) semi-circular ribs case at H = 66mm and 400 RPM

The comparison of velocity contour plots for swirl flow plain, square ribs, and semi-circular ribs cases have been shown in Figure 5.12 for 500 RPM at height H = 96mm. The velocity for all the mentioned cases almost follows the same trend as previous compared results.

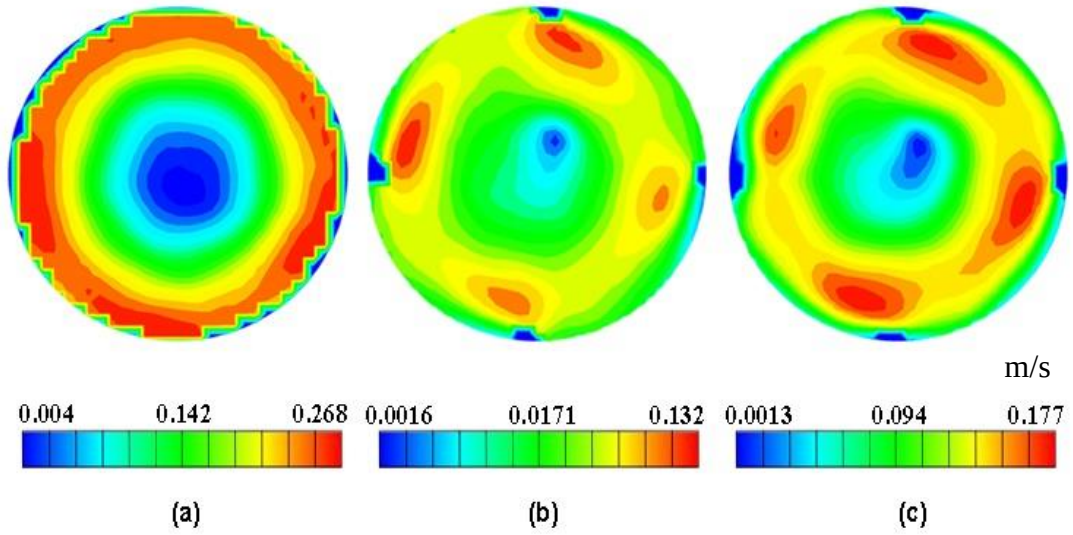

Figure 5.12: Comparison of velocity contours for a) swirl flow plain, b) square ribs, and c) semi-circular ribs case at H = 96mm and 500 RPM

In the comparison of velocity contours for all the cases, the velocity is minimum near the center of the cylinder. The flow behavior of particles at the center is such that they resist each other due to opposite rotation which causes almost zero velocity. Wall friction can be seen in all above-mentioned cases as highly visible due to which velocity approaches zero.

5.3 Vorticity

The local rotation or curl of the 3D velocity distribution at a given position is referred to as vorticity. In Figure 5.13, the contours of vorticity for swirl flow plain case, vorticity around square ribs, and semi-circular ribs are shown. In each case, negative vorticity is seen near the center of the cylinder. Vorticity is the maximum near cylinder wall for swirl flow plain case. The highest positive values of vorticity are indicated in the recirculation zone downstream of the ribs. The separation and reattachment of the flow, as well as the formation of vortices surrounding the rib, cause this vorticity development [1].

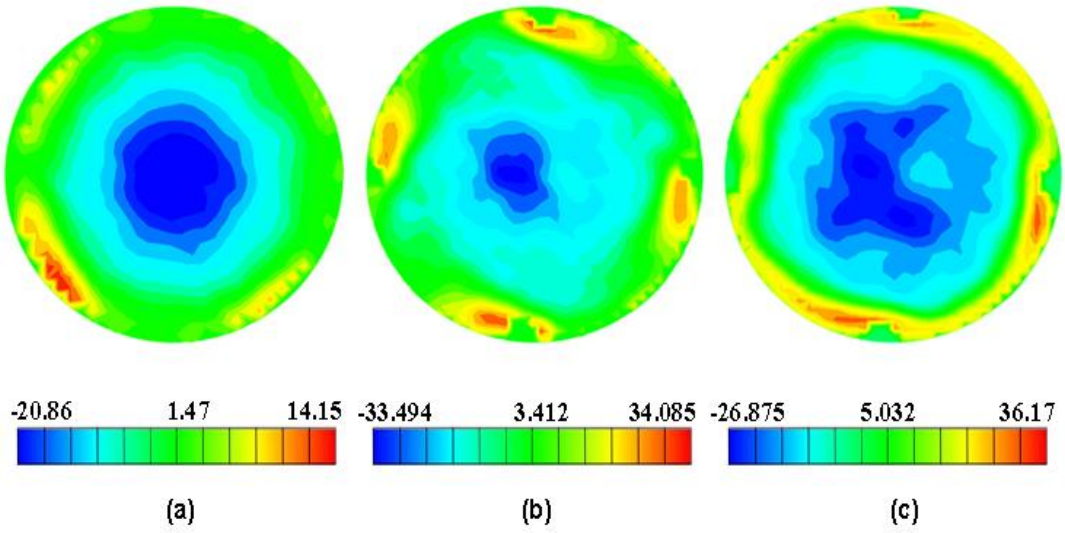

Figure 5.13: Vorticity contours for swirl flow a) plain case b) square ribs case c) semi-circular case at H = 36mm and 400 RPM

In ribbed cases, both rib shapes show almost the same behavior and the number of swirls is equal to the number of ribs in each case. Ribbed cylinders show four swirls in each case. One can say that the increase in the number of swirls can cause more mixing due to the chaotic and turbulent behavior of flow particles. The semi-circular ribs case has more velocity and vorticity value, so it has more mixing than the square ribs case.

5.4 Swirl Strength

Swirl strength is defined as the imaginary component of the complex eigen value of the velocity gradient tensor J.

Gradients in the z-direction cannot be determined for planar data, therefore reducing them to zero makes eigen value computation easier, allowing the square of the imaginary part to be computed as (equation 5.1):

$$\lambda_{ci}^2 = \frac{1}{4}\left(\frac{\partial U}{\partial x}\right)^2 + \frac{1}{4}\left(\frac{\partial V}{\partial y}\right)^2 - \frac{1}{2}\frac{\partial U}{\partial x}\frac{\partial V}{\partial y} + \frac{\partial V}{\partial x}\frac{\partial U}{\partial y} \quad \ldots\ldots\ldots (5.1)$$

-which is the number known as the swirl strength [2].

The swirl strength contours for the plain case, square ribs case, and semi-circular ribs cases at H = 66mm and 400 RPM are shown in Figure 5.14. The swirl strength for the plain case is maximum close to the cylinder wall and for square ribs and semi-circular ribs cases, it is maximum before and after the ribs. Swirl strength is minimum near the center of the cylinder for all compared cases.

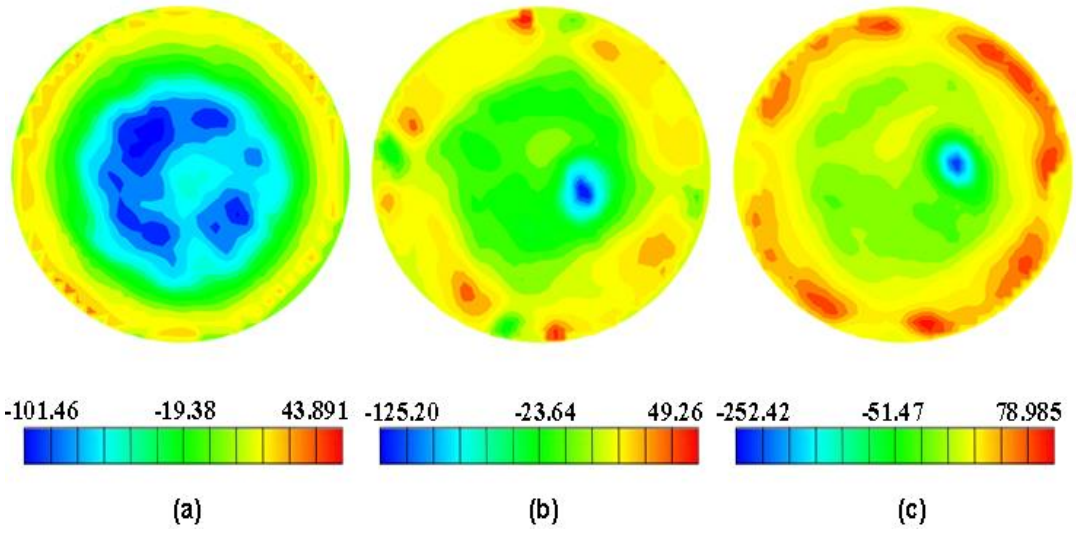

Figure 5.14: Swirl strength contours for swirl flow a) plain case b) square ribs case c) semi-circular case at H = 66mm and 400 RPM

Summary

In this chapter, a detailed description of the results of the swirl flow system has been discussed. The velocity vs radius profile plots for swirl flow plain, square ribs, and semi-circular ribs cases have been compared. Similarly, the comparison of velocity contours has been made. The contour plots of vorticity and swirl strength have also been compared.

References

[1] V. P. Fragos, S. P. Psychoudaki, and N. A. Malamataris, “Two-dimensional numerical simulation of vortex shedding and flapping motion of turbulent flow around a rib,” Comput. Fluids, vol. 69, pp. 108–121, 2012.

[2] R. J. Adrian, K. T. Christensen, and Z. C. Liu, “Analysis and interpretation of instantaneous turbulent velocity fields,” Exp. Fluids, vol. 29, no. 3, pp. 275–290, 2000.

Chapter 6 : Conclusions and Recommendations

6.1 Conclusions

In this study, an experimental investigation of swirl flow and mixing was carried out in a turbulent range using PIV. Experiments were carried out in cylinders first with a swirl flow plain case, and then with square, and semi-circular ribs. RPMs considered for the experiment were 300, 400, and 500. The effect of square and semi-circular ribs on turbulence was studied for velocity, vorticity, and swirl strength. Velocity contours and velocity profile plots were extracted and presented in this research.

1. From velocity contours, it can be seen that the velocity gradually increases outwards from the center of the cylinder in swirl flow plain, square and semi-circular rib cases. Also, the velocity increases with the increase in RPM. Velocity approaches nearly zero close to the cylinder walls due to wall friction.
2. Negative vorticity was observed near the center of the cylinder in all cases. Maximum vorticity was observed close to the cylinder wall for the plain case. Positive vorticity values were highest in the recirculation zone downstream of the semi-circular rib.
3. The swirl strength for the plain case was maximum near the cylinder wall and for the square and semi-circular rib cases, it was maximum before and after the ribs.
4. In semi-circular ribs, turbulence increases due to an increase in vorticity and swirl strength. Moreover, its velocity is greater than the square ribs case. Hence it results in better mixing.

6.2 Recommendations

Based on this study, different recommendations are given in this section. Different types of work can be done in the future to study swirl flow more effectively.

- Ribs installed at different angles can be investigated.
- Different shapes of ribs can be studied to understand the effect on the degree of swirl and mixing of particles in any fluid. Like C channel rib, star rib, and triangular rib.
- Swing in direction of rotation on the impact of swirl flow can be studied, in clockwise and anticlockwise directions after a certain interval of time.
- Different shapes of cylinders can be used, like funnel shapes, star shape cylinders, etc.
- Viscous liquids like glycerine can be used to study the effect on swirl flow.

Acknowledgements

All praise be to Allah and peace and blessings be upon our Prophet Muhammad (peace be upon him). His favors enabled me to conduct this work, without which it would not have been possible.

I would like to acknowledge the continuous support and love from my parents and siblings during the entire degree program.

I would like to acknowledge the supervision and guidance received from Dr. Majid Ali throughout this research work. His supervision and motivation kept me glued to the topic till the end. His guidance helped me during the time of research and writing of this thesis. His valuable recommendations and support made this work to be complete.

My sincere gratitude also goes to my co-supervisor Dr. M. Israr Siddiqui for his continuous supervision and moral and technical support during the fabrication process and experimental work. Whenever I was stuck during this research work, his wisdom and experience made it possible for me to cope with the issue. He deserves my sincere gratitude because of his constant kindness, motivation, enthusiasm, and immense knowledge.

I would like to extend my best regards to GEC members for their encouragement, insightful comments, and hard questions regarding the project.

I am grateful to Laboratory Engineer Mr. Hassan Nazir for his technical assistance. I would also acknowledge the Thermal Energy Laboratory of USPCAS-E (NUST) for providing me the space to conduct my research peacefully and efficiently. I also acknowledge the help and support of my fellow students for keeping me intact during the research.

Last but not the least, I would like to thank my friends Nadeem Mohsin, Waseem Shehzad, Muhammad Umar Iqtidar, and Muhammad Hamza Saeed for the stimulating discussions which helped me during the research work.

Appendix A: Research Publications

Conference: 6th International conference on **Energy, Environment, and Sustainable Development 2022 (EESD 2022).**

Title: Experimental study of swirl flow in a cylindrical container using Particle Image Velocimetry.

Authors: Tahir Javed, M. Israr Siddiqui, Majid Ali.

Abstract:

The current study demonstrates an experimental investigation of swirl flow and mixing employing Particle Image Velocimetry (PIV) within the turbulent range. Swirl flow is produced when the axial flow is provided with a tangential component of velocity. Swirl flow enhances mixing, improves heat conduction, and is used for separation by centrifugation. The experiments were carried out in a glass cylinder with and without ribs. The RPMs used were 300, 400, and 500. The effect of ribs on turbulence was studied for velocity, vorticity, and swirl strength. The results show that with the increase in velocity, turbulence also increases, hence better mixing. Also, with the installation of square ribs in the cylinder, the mixing is enhanced.

Keywords: Swirl Flow; Mixing; PIV; Square Ribs.

Submitted: November 25, 2021

Accepted: December 06, 2021

Presented: January 18, 2022.